PHYSICAL REVIEW A **68**, 012703 (2003)

Unified theoretical treatment of dissociative recombination of D_{3h} triatomic ions: Application to H_3^+ and D_3^+

Viatcheslav Kokoouline and Chris H. Greene
Department of Physics and JILA, University of Colorado, Boulder, Colorado 80309-0440, USA

(Received 14 March 2003; published 9 July 2003)

The dissociative recombination of an H_3^+ ion after it is struck by a low-energy electron is important for understanding observations of H_3^+ in diffuse interstellar clouds. At the same time, it is the simplest triatomic ion and for this reason its theoretical description can serve as a prototype for other polyatomic ions. Meanwhile, experimental determinations of the recombination rate have varied widely, which has resulted in some controversy and confusion. Until recently, it seemed unlikely that this problem could be resolved by theoretical studies because the mechanism of H_3^+ dissociative recombination remained unclear. A recent study, however [Kokoouline *et al.*, Nature (London) **412**, 891 (2001)], provided evidence that the inclusion of the Jahn-Teller coupling can produce a dissociative recombination rate that overlaps the range of experimental observations. Here, we propose a theoretical description of the coupling between nuclear and electronic degrees of freedom in a polyatomic molecule, which describes the competition between autoionization and predissociation of the Rydberg states formed after an incident electron is captured. The method treats the vibrational and rotational excitations of the ion, accounts for all symmetry restrictions imposed by the geometry of the molecule, including vibrational, rotational, and electronic and nuclear-spin symmetries. The framework combines the multichannel quantum-defect theory, the adiabatic hyperspherical approach, and the techniques of outgoing-wave Siegert pseudostates. The proposed method can be applied to studies of dissociative recombination of other triatomic ions, including all the degrees of freedom quantum mechanically. Our calculations of the cross section and the recombination rate confirm that the Jahn-Teller effect is responsible for the large rate in H_3^+. Theoretical results for dissociative recombination of H_3^+ are in agreement with storage-ring experiments.

DOI: 10.1103/PhysRevA.68.012703 PACS number(s): 34.80.Ht, 34.80.Kw, 34.80.Lx

I. INTRODUCTION

Over the past two decades, the process of dissociative recombination (DR)

$$H_3^+ + e^- \rightarrow H_2 + H \quad \text{or} \quad H + H + H \tag{1}$$

of the triatomic hydrogen ion H_3^+ has attracted extensive attention from both experiment and theory. This process is of practical importance in astrophysics because the ion acts as a proton donor in chemical reactions that occur in interstellar clouds. It is also important because it is the simplest triatomic ion, and it consequently serves as a key meeting point for theoretical and experimental efforts to understand polyatomic DR processes. We refer the reader to a number of recent review papers [1–6] that summarize the ongoing problems which have arisen from seemingly contradictory studies of dissociative recombination in this species.

The goal of the present study is to describe a theoretical method that can describe DR in triatomic molecules, including the full, three-dimensional motion of the rotating, vibrating, and dissociating nuclei. The recognition that the Jahn-Teller coupling controls the interaction between the incident electron and the vibrating H_3^+ nuclei has stimulated our effects in developing this method. We have attempted to make the theoretical description as robust and reliable as the present-day description of dissociative recombination in diatomic molecules [7–15]. A reader well versed in DR theory may find our approach unconventional, because we combine disparate theoretical elements that have not been used in this particular combination before. Accordingly, along the way we will provide evidence that the approximations introduced are physically sensible and mathematically tractable. The present study is meant to be fully self-contained, which has required a much lengthier presentation than the preliminary account discussed in Ref. [16].

The problems that have hindered a full description of DR in H_3^+ to date can be summarized as follows.

(1) In contrast to diatomics, the vibrational degrees of freedom have three dimensions. This alone has proved to be a significant barrier, since essentially all previous theories have been forced to treat the vibrational degrees of freedom with models of reduced dimensionality.

(2) Partly as a corollary of problem (1), symmetry-breaking Jahn-Teller effects have not been treated, even though evidence existed from H_3 photoabsorption studies [17,18] that the Jahn-Teller mechanism provided the conduit for the strongest coupling between electronic and vibrational degrees of freedom.

(3) The lone dissociative electronic surfaces of H_3 which are energetically accessible at low-energy fail to cross the ground-state ionic potential surface, which was believed in the past to result in very low DR rates. This makes it even more important to develop a theoretical method that can correctly describe indirect recombination via intermediate Rydberg state pathways. The importance of the intermediate Rydberg states for H_3^+ DR was suggested in recent theoretical studies on predissociation of H_3 states [4,19–21].

(4) For the techniques most successful in treating the complicated Rydberg state interactions, namely, those of multichannel quantum-defect theory (MQDT), it is still chal-

lenging to incorporate dissociative channels. This is the case even though there has been a significant progress along these lines, mostly through the work of Jungen [9,11,13–15] and Suzor-Weiner [7–9].

(5) Rotational degrees of freedom, almost always neglected in DR calculations, even for diatomics, could play a significant role in H_3^+. Rotation could be important because DR is thought to hinge on the time reverse of autoionization—the capture of an incident electron into a Rydberg state—and because rotational autoionization provides the broadest autoionization widths observed to date in H_3 Rydberg states.

Our approach to deal with these five problems combines theoretical elements that have not previously been unified. To be specific, hyperspherical coordinate techniques have been applied with increasing frequency and success in recent years [22–27] to describe vibrational excitations and two-body or three-body dissociation of triatomics. Yet the application of hyperspherical methods to describe the coupling between an incident electron and the vibrational or dissociative degrees of freedom has apparently not been considered previously. We show that it can be carried out, and that it permits a natural inclusion of the Jahn-Teller coupling. Our detailed calculations confirm that the dissociative recombination of H_3^+ is controlled by the Jahn-Teller mechanism, in agreement with a recent suggestion and estimate [28]. Finally, we adapt a recently proposed method [29] that utilizes vibrational channel functions obeying Siegert pseudostate boundary conditions to describe the nonperturbative coupling between ionization and dissociation channels.

The theoretical description of the DR process in H_3^+ is complicated by several factors. The only possible dissociative channels in the energy range of interest are associated with the ground electronic state of the neutral triatomic molecule. The potential surface of this state does not cross the ionic potential surface. The resulting small overlap of the neutral and ionic nuclear wave functions would suggest a relatively slow DR rate, inconsistent with the fast dissociation observed in storage-ring experiments. Another complication results from the necessity to treat three-dimensional vibrational dynamics of the ion and the neutral molecule. Moreover, one should include many coupled potential surfaces corresponding to the $H_3^+ + e^-$ system with various Rydberg states of the neutral molecule. Finally, the rotation of the ion should be included in order to try to understand the disagreements among different experiments, where rotation may or may not play a key role.

A number of techniques have been developed to treat dissociative recombination of a diatomic molecule. Whereas direct processes can be described using a treatment developed by O'Malley [30], methods that include indirect pathways are primarily based on MQDT. [11,13,31] MQDT applications have successfully described the coupling of many coupled Rydberg, ionization, and dissociative channels, including rotational excitations. MQDT has also been used to treat the competition between autoionization and predissociation of Rydberg states. At first glance, however, the presence of three internuclear distances instead of one renders these techniques inapplicable to the e-H_3^+ collision. This is because a crucial factor of these techniques is the existence of only one adiabatic coordinate, namely, the internuclear distance.

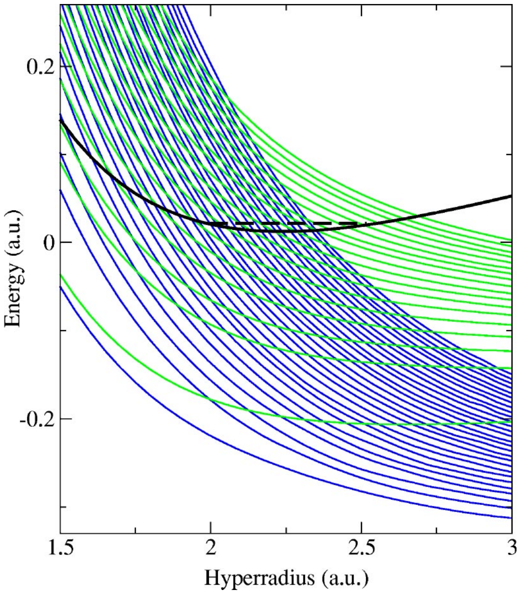

FIG. 1. The problem of DR of H_3^+ in the hyperspherical adiabatic approximation. The lowest hyperspherical adiabatic potential (thick full line) of the H_3^+ and number of hyperspherical adiabatic potentials of the neutral molecule (thin lines). Lower family of lines (darker lines) dissociate to the H_2+H channel; the upper family (lighter lines) dissociate to the $H+H+H$ channel. To calculate hyperspherical adiabatic curves we used the three-dimensional H_3^+ potential from Ref. [48] and the H_3 potential from Refs. [35–37]. Since the density of hyperspherical states is high, only every tenth H_3 potential curve is shown in the figure. The dashed line shows the position of the ground vibrational level of the ion, which is the only one populated in the relevant experiments.

In this situation the hyperspherical adiabatic approach [32], applied extensively to triatomic systems during the last decade [23,33,34], seems well suited to fit DR of H_3^+ into the familiar framework of dissociative recombination of diatomic ions. In our treatment the only adiabatic vibrational coordinate is the hyperradius. To demonstrate the simplicity and the similarity of the problem to the diatomic case, Fig. 1 presents the lowest hyperspherical adiabatic potential of H_3^+, and a number of adiabatic hyperspherical potential curves of the neutral molecule. (The neutral curves are calculated using the *ab initio* three-dimensional H_3 potential from Refs. [35–37].) The dashed line shows the position of the ground vibrational level of the ion, which is the only vibrational level populated in the relevant experiments. The neutral states are seen to cross the ionic potential, giving rise to a nonzero vibrational overlap. After viewing this picture, and after realizing that the neutral hyperspherical potential curves that lie energetically above the ionic ground-state potential curve will have a nonzero imaginary part reflecting the possibility of autoionization occurring at that value of R, one sees that the usual O'Malley-type diatomic DR methods can now describe DR for H_3^+, except that the internuclear distance is replaced by the hyperradius. This is the crudest level of approximation, adopted to estimate the ‘‘direct’’ DR rate in Ref. [28]. Even though the more accurate MQDT-based approach developed in this paper does not use that O’Malley-type methodology, it is still useful for qualitatively visualizing the way recombinative capture of the electron takes place. For more complex systems, however, where the level of resonance-by-resonance detail pursued in the present study is unnecessary or unfeasible, this approximate technique may be a useful way to proceed.

The use of the hyperspherical adiabatic method significantly simplifies the treatment but it fails to account for the reason that why previous theoretical efforts were unable to explain the large DR rate observed in storage-ring experiments. A resolution of this discrepancy requires understanding the role of the Jahn-Teller effect in the electron-H_3^+ coupling [28]. The full *ab initio* inclusion of this Jahn-Teller coupling, through an extension of the work of Staib and Domcke [38,39] and of Stephens and Greene [17,18] is a second vital element of our treatment.

Our previous paper [28] estimated lower and upper limits for dissociative recombination of the rotationless ion. The lower limit assumes that only direct paths to dissociation contribute to the DR rate, because all Rydberg states are assumed to autoionize back to the electron-ion complex. The upper limit refers to a calculation carried out under the assumption that electron capture into a Rydberg state resonance ultimately leads to predissociation, without any loss due to autoionization. In the present paper, we consider the competitive character of predissociation and autoionization once a Rydberg state is populated. Such a competitive character was successfully incorporated into a description of diatomic molecules in studies by Giusti [7] and by Jungen and coworkers [10,13–15], but it has never been able to describe dissociative channles for triatomics. In principle, the adiabatic hyperspherical approximation reduces the problem of H_3^+ DR to a model, for which one of the two mentioned approaches—that of Jungen or Giusti—can be applied. However, because of a large number of hyperspherical channels, such an approach is difficult to implement in the present problem. Having initially attempted to use Giusti’s approach, we have finally chosen to employ a different approach for the description of the competition between ionization and dissociation [29].

The paper is organized as follows. In the following section, we review the relevant symmetry properties of the H_3^+ ion. We consider transformations of rotational, vibrational, and nuclear-spin wave functions of the ion under operations from the symmetry group of H_3^+. Section III is devoted to a discussion of the Jahn-Teller coupling in H_3^+. Section IV describes the way vibrational motion of H_3^+ is incorporated into the present approach. We use the adiabatic hyperspherical approach to handle vibrational dynamics of the three nuclei. Section V describes the treatment of dissociative channels. The treatment employs outgoing Siegert states in the dissociative channels. In Sec. VI, we construct the total wave function of the $H_3^+ + e^-$ complex and calculate the total scattering matrix for collisions between the ion and the electron. For this goal we use frame-transformation techniques [11,13,31,40]. In Sec. VII, we present calculations of the DR cross section and rate. We discuss different schemes of energy averaging over different degrees of freedom relevant to different conditions in experiments. Section VIII discusses the results. Section IX is devoted to a DR calculation for D_3^+. We briefly discuss the similarities and the differences between the H_3^+ and D_3^+ ions and we compare our results with existing experimental observations. Finally, Sec. X presents our conclusion.

II. SYMMETRY OF THE H_3^+ ION

Although the symmetry of the H_3^+ ion has been discussed many times (see, for example, the work of Bunker and Jensen [41] or Ref. [42]), we believe that a brief description of the symmetry issues related to the problem will be useful in order to make the following theoretical development more self-contained.

The total Hamiltonian of H_3^+ commutes with all operations [41]: translation of the ion along a space-fixed direction; rotation of the ion about a space-fixed axis passing through the center of mass of the ion; permutation of space and spin coordinates of the electrons; permutation of the space and spin coordinates of the nuclei; and inversion of the coordinates of all the particles of the ion through the center of mass. As a result, the full Hamiltonian group G_{full} can be written as a direct product of groups corresponding to the above symmetry operations:

$$G_{full}=G_T\otimes K_s\otimes S^{(e)}\otimes G^{CNPI}, \tag{2}$$

where G_T is the symmetry group of pure translations of the ion, K_s is the rotational group, $S^{(e)}$ is the group of electron permutation, and G^{CNPI} is the group including permutation of nuclei and total inversion. The effect and the meaning of the translation group is trivial in our case. Since we consider only the singlet electronic ground state $1s^2$ of the ion, the operations of electron permutation are also trivial. Thus, we consider here only the symmetry operations associated with the product of the following two groups:

$$G_f=K_s\otimes G^{CNPI}. \tag{3}$$

The complete nuclear permutation-inversion (CNPI) group of H_3^+ is $D_{3h}(M)$ and it includes 12 elements [41,42]. For the lower excited rovibrational states of H_3^+, the rotational and vibrational motions remain uncoupled. The interaction of the nuclear spin with spatial motion is known to be very weak. Therefore, every operation $\mathcal{O}$ from $D_{3h}(M)$ can be cast as a product of three operations: nuclear-spin permutation P_I, a rotation $\mathbf{R}$, and a permutation of spatial displacements of nuclei from the symmetric configuration, P_Q: $\mathcal{O}=\mathcal{O}(I)\mathcal{O}(\mathbf{R})\mathcal{O}(\mathcal{Q})$. Table I summarizes the relations between $\mathcal{O}$ and $\mathcal{O}(I)\mathcal{O}(\mathbf{R})\mathcal{O}(\mathcal{Q})$ for all the elements of the $D_{3h}(M)$ group [41,42].

The total wave function $\Phi_t^{n.sym}$ of the ion can thus be represented as a product of three parts,

TABLE I. This table demonstrates the effect of operations from the CNPI group of $H_3{}^+$, $D_{3h}(M)$ group. Every $D_{3h}(M)$ operation is recast as a product of three operations acting as elements of (1) the molecular point group D_{3h}, (2) the molecular rotation group (equivalent rotations), and (3) nuclear-spin permutation group S_3. For the elements of equivalent rotation, we adopt the notation of Bunker and Jensen [41], where R_a^α means a rotation through angle α about the axis a. Elements ρ_i of the nuclear-spin permutation group S_3 act just as ordinary permutations of the nuclear-spin projections ($m_I = \pm 1/2$) on the molecule-fixed axis *z*. We choose molecular coordinate axes as shown in Fig. 3. Only six elements of the $D_{3h}(M)$ group are shown in the table. The remaining six operations are obtained from those already specified.

$D_{3h}(M)$:	E	(123)	(12)	E^*	(123)*	(12)*
Point group D_{3h}	E	C_3	C_2	σ_h	$C_3\sigma_h$	σ_v
Equivalent rotation	R^0	$R_z^{2\pi/3}$	R_x^π	R_z^π	$R_z^{-\pi/3}$	R_y^π
Nuclear-spin permutation	ρ_0	ρ_{123}	ρ_{12}	ρ_0	ρ_{123}	ρ_{12}

$$\Phi_t^{n.sym} = \Phi_I \mathcal{R}(\alpha,\beta,\gamma)\Phi_{\mathbf{v}}(\mathcal{Q}). \tag{4}$$

Here α,β,γ are the three Euler angles defining the orientation of the molecule-fixed axis with respect to the space-fixed coordinate system. $\mathcal{Q}$ is the triad of coordinates describing internuclear distances. Our goal is to construct the elements of the product on the right-hand side of Eq. (4) and to determine how these products transform under the symmetry operations of $D_{3h}(M)$.

The rotational part $\Phi_R(\alpha,\beta,\gamma)$ of the total wave function for the $H_3{}^+$ is taken to be a symmetric top wave function, in our level of approximation. (This should be adequate at comparatively small internuclear distances where we anticipate the capture process occurs, and where the pathway is chosen between preionization and predissociation.)

$$\mathcal{R}(\alpha,\beta,\gamma) = |N^+,K^+,m^+\rangle = \left[\frac{2N^+ + 1}{8\pi^2}\right]^{1/2} [D^{N^+}_{m^+,K^+}(\alpha,\beta,\gamma)]^*. \tag{5}$$

Table II gives the transformations of the rotational function under elements of the rotational subgroup of $D_{3h}(M)$. The phase of the Wigner function is chosen as by Varshalovich *et al.* in Ref. [43].

Vibrational wave functions

$$\Phi_{\mathbf{v}}(\mathcal{Q}) = |v_1, v_2^{l_2}\rangle \tag{6}$$

of the ion are specified by the triad of quantum numbers $v_1, v_2^{l_2}$. The quantum number v_1 describes the symmetric stretch mode, which of course preserves the equilateral configuration (C_{3v}) of the ion. The value of v_2 indicates the number of asymmetric radial vibrational quanta. Finally, the quantum number l_2 measures the angular momentum about the main symmetry axis of the molecule, generated by vibration [44]. l_2 can have values $-v_2, -v_2+2, \ldots, v_2-2, v_2$.

The significance of negative l_2 is that for states with $l_2 \neq 3\tilde{k}$ (here and below, $\tilde{k}$ is an arbitrary integer number), the pair of functions $|v_1, v_2^{-l_2}\rangle$, $|v_1, v_2^{l_2}\rangle$ correspond to two states with opposite senses of vibrational rotation. Both $|v_1, v_2^{\pm l_2}\rangle$ with $l_2 \neq 3\tilde{k}$ have the same vibrational energy and transform according to the two-dimensional E representation of the vibrational subgroup of D_{3h} [41]. The states with $l_2 = 0$ are always of A_1 symmetry. The states with $l_2 = 3\tilde{k}$, but $l_2 \neq 0$, can be of A_1 or A_2 symmetry. In order to avoid introduction of one more index distinguishing the A_1 or A_2 states with $l_2 = 3\tilde{k}$, $l_2 \neq 0$, we give a positive l_2 number to A_1 states, and a negative one to A_2 states. With this convention about l_2 labels, the effect of the symmetry operations of the vibrational function are specified in Table III. We would like to note that actual values of v_2 and l_2 are not used in our treatment. We need to know only properties of a given vibrational function with respect to permutation operations, i.e., we need to know only what is the symmetry of the function. Moreover, the indices v_2 and l_2 are becoming very approximate for higher vibrational excitations. In contrast, the symmetry of the vibrational function can always be identified.

In the present treatment, the mutual phase of degenerate states $|v_1, v_2^{l_2}\rangle$ with $l_2 \neq 3\tilde{k}$ is handled with slight differences from the convention of Refs. [44,45]. This is done to obtain vibrational wave functions that transform exactly as $|N^+,K^+,m^+\rangle$ under operations from $D_{3h}(M)$. Transformations of $|v_1, v_2^{l_2}\rangle$ with the present choice of phases is given by Table III. Using the present convention, the Hougen quantum number [44,45] is $g = k + l_2$.

The third part of the total ionic wave function is the nuclear-spin wave function. It is constructed in the following way. Every proton in the ion can be in one of the two nuclear-spin states

$$\alpha = |i = \tfrac{1}{2}, m_i = \tfrac{1}{2}\rangle$$

or

$$\beta = |i = \tfrac{1}{2}, m_i = -\tfrac{1}{2}\rangle \tag{7}$$

TABLE II. Transformations of the rotational symmetric-top wave function $|N^+,K^+,m^+\rangle$ under elements of the $D_{3h}(M)$ group. Since the quantum numbers N^+ and m^+ are not affected by the operations, they are not specified in the result. All transformations, here and throughout this paper, are passive. In this table and below, $\omega = e^{i\pi/3}$.

Equivalent rotation $\mathcal{O}_{\mathbf{R}}$:	R^0	$R_z^{2\pi/3}$	R_x^π	R_z^π	$R_z^{-\pi/3}$	R_y^π
$\mathcal{O}(\mathbf{R})\|N^+,K^+,m^+\rangle$	$\|K^+\rangle$	$\omega^{2K^+}\|K^+\rangle$	$(-1)^{N^+}\|-K^+\rangle$	$(-1)^{K^+}\|K^+\rangle$	$\omega^{-K^+}\|K^+\rangle$	$(-1)^{N^+ + K^+}\|-K^+\rangle$

TABLE III. Transformations of the vibrational wave function $|v_1,v_2^{l_2}\rangle$ under elements of the D_{3h} point group. Since vibrations of $H_3{}^+$ always occur within the plane, the vibrational functions $|v_1,v_2^{l_2}\rangle$ transform as elements of the C_{3v} subgroup of the D_{3h} point group, $D_{3h}=\sigma_h\otimes C_{3v}$. Therefore, the operation σ_h leaves the vibrational states unchanged. In the table, the index s_2 is 1 for all states except A_2 states, for which it is -1. The index $l_2'=l_2$ for all states with $l_2=0\ (\mathrm{mod}\,3)$, and $l_2'=-l_2$ for $l_2=1,2\ (\mathrm{mod}\,3)$.

Point group D_{3h}:	E	C_3	C_2	σ_h	$C_3\sigma_h$	σ_v
$\mathcal{O}(\mathcal{Q})\|v_1,v_2^{l_2}\rangle$	$\|v_1,v_2^{l_2}\rangle$	$\omega^{2l_2}\|v_1,v_2^{l_2}\rangle$	$s_2\|v_1,v_2^{l_2'}\rangle$	$\|v_1,v_2^{l_2}\rangle$	$\omega^{2l_2}\|v_1,v_2^{l_2}\rangle$	$s_2\|v_1,v_2^{l_2'}\rangle$

where i is the spin of proton and m_i is its projection on the molecular symmetry axis (z). The primitive nuclear-spin wave function is constructed as a product of the individual spin states for each proton. Each spin wave function of the three nuclei must be a linear combination of the following:

$$|\alpha\alpha\alpha\rangle,$$

$$|\alpha\alpha\beta\rangle,|\alpha\beta\alpha\rangle,|\beta\alpha\alpha\rangle,$$

$$|\beta\beta\alpha\rangle,|\beta\alpha\beta\rangle,|\alpha\beta\beta\rangle,$$

$$|\beta\beta\beta\rangle. \tag{8}$$

The ordering of substates within each ket is important in Eqs. (8). Our convention is that the first position in each product corresponds to the state of proton number 1 in Fig. 3, the second position is that of proton 2, and the third position is that of proton 3. From these combinations we want to construct nuclear-spin wave functions that transform in the same way as the vibrational and rotational wave functions determined above. Since permutations of the three protons constitute a reducible representation of the S_3 permutation group, we proceed in the standard way. Specifically, we construct the A and E spin irreducible representations, which transform as follows under permutations:

$$\Phi_A^I(M=3/2)=|\alpha\alpha\alpha\rangle,$$

$$\Phi_A^I(M=1/2)=\frac{1}{\sqrt{3}}(|\alpha\alpha\beta\rangle+|\alpha\beta\alpha\rangle+|\beta\alpha\alpha\rangle),$$

$$\Phi_{E_a}^I(M=1/2)=\frac{1}{\sqrt{6}}(2|\alpha\alpha\beta\rangle-|\alpha\beta\alpha\rangle-|\beta\alpha\alpha\rangle),$$

$$\Phi_{E_b}^I(M=1/2)=\frac{1}{\sqrt{2}}(|\alpha\beta\alpha\rangle-|\beta\alpha\alpha\rangle). \tag{9}$$

In the same way, functions A and E are constructed for $M=-3/2$ and $M=-1/2$. The functions Φ_A^I are totally symmetric under all permutations (A representation). By direct application of the transformation matrices of the S_3 operations, one can verify that these combinations transform under nuclear permutations according to the A and E irreducible representations. For instance, the operations (12) and (123) act on Φ_E^I functions as the following:

$$\rho_{12}\Phi_{E_a}^I=\Phi_{E_a}^I,$$

$$\rho_{12}\Phi_{E_b}^I=-\Phi_{E_b}^I,$$

$$\rho_{123}\Phi_{E_a}^I=-\frac{1}{2}\Phi_{E_a}^I-\frac{\sqrt{3}}{2}\Phi_{E_b}^I,$$

$$\rho_{123}\Phi_{E_b}^I=\frac{\sqrt{3}}{2}\Phi_{E_a}^I-\frac{1}{2}\Phi_{E_b}^I. \tag{10}$$

For the product of Eq. (4) we need the following functions:

$$\Phi_0^I(M=3/2)=\Phi_A^I(M=3/2),$$

$$\Phi_0^I(M=1/2)=\Phi_A^I(M=1/2),$$

$$\Phi_{\pm1}^I(M=1/2)=\Phi_{E_a}^I(M=1/2)\pm i\Phi_{E_b}^I(M=1/2). \tag{11}$$

It can be shown that states $\Phi_0^I(M=3/2)$ and $\Phi_0^I(M=1/2)$ are states with the total nuclear-spin $I=3/2$ (ortho states) and states $\Phi_{\pm1}^I(M=1/2)$ have nuclear-spin $I=1/2$ (para states). We will be referring uniformly to the states of Eq. (11) as $\Phi_{g_I}^I$, where $g_I=0$ or ±1. Thus, these states are characterized by two quantum numbers I and M_I. The third quantum number g_I is determined by I.

Using Eqs. (9), (11), and (10) we determine transformations of states (11) under the nuclear permutations. The results are summarized in Table IV.

Having established the transformation properties of each individual part of the product wave function in Eq. (4), we next consider transformations of the whole product. Consider again operations (12) and (123),

$$(123)\Phi_t^{n.sym}=\omega^{2(K^++l_2+g_I)}\Phi_t^{n.sym},$$

$$(12)\Phi_t^{n.sym}(K^+,l_2,g_I)=(-1)^{N^+}s_2\Phi_t^{n.sym}(-K^+,l_2',-g_I). \tag{12}$$

TABLE IV. Transformations of the nuclear-spin states under nuclear permutations.

Nuclear-spin permutation $\mathcal{O}(I)$	ρ_0	ρ_{123}	ρ_{12}
$\mathcal{O}(I)\Phi_{g_I}^I$	$\Phi_{g_I}^I$	$\omega^{2g_I}\Phi_{g_I}^I$	$\Phi_{-g_I}^I$

In the second equation, the quantum numbers K^+, l_2, and g_I are explicitly specified because they are changed by (12). Since the total ionic eigenfunction should be antisymmetric under (12) we determine Φ_t,

$$\Phi_t=\frac{1}{\sqrt{2}}[\Phi_t^{n.sym}(K^+,l_2,g_I) -(-1)^{N^+}s_2\Phi_t^{n.sym}(-K^+,l_2',-g_I)]. \qquad (13)$$

The condition of antisymmetry under (12) is explicitly enforced. The wave function must be totally antisymmetric under all such binary permutations, which is possible only if Φ_t transforms according to either the A_2' or A_2'' representation of the $D_{3h}(M)$ group. This requires that $\omega^{2(K^+ + l_2 + g_I)}=1$, which can be interpreted as $\tilde{G}=3\tilde{k}$, where $\tilde{G}=K^+ + l_2 + g_I$. The parity of the total state, which is determined as the transformational property under the E^* operation, is determined by K^+: the parity is even or odd as K^+ is even or odd, respectively.

We next consider in detail the ortho nuclear-spin states. For ortho ($I=3/2$) states, $g_I=0$ and the nuclear-spin factors are identical for both components of the sum in Eq. (13). Consequently, a simplified expression results, namely,

$$\Phi_t^{rv}=\frac{1}{\sqrt{2}}[|N^+,K^+,m^+\rangle|v_1,v_2^{l_2}\rangle -(-1)^{N^+}s_2|N^+,-K^+,m^+\rangle|v_1,v_2^{l_2'}\rangle]. \qquad (14)$$

Only states with $\tilde{G}=3\tilde{k}$ are allowed. $\tilde{G}$ is reduced now to $\tilde{G}=K^+ + l_2$ that coincides the Hougen quantum number g [44] for $I=3/2$. Note that for the ground vibrational state $(v_1,v_2,l_2)=0$, the rotational level $N^+,K^+=0$ does not exist since $\Phi_t^{rv}\equiv 0$. The total symmetry of the state is A_2' or A_2'' depending on whether K^+ is even or odd.

For para states, the nuclear-spin part of the wave function cannot be factored out. The lowest ortho levels are $A_2'\{00^0\}(10)$ and $A_2''\{00^0\}(33)$, whereas the lowest para levels are $A_1'\{00^0\}(22)$ and $A_1''\{00^0\}(11)$.

III. THE JAHN-TELLER EFFECT FOR H_3

The Jahn-Teller coupling is a generic non-Born-Oppenheimer effect in polyatomic molecules having D_{3h} or higher total symmetry [46]. Basically, there are two degenerate electronic states at the equilateral geometry of nuclei (C_{3v} nuclear symmetry). For any distortion away from this symmetry, the electronic degeneracy is split and the electronic states acquire different energies. This is the Jahn-Teller effect. When the D_{3h} molecule vibrates, the Jahn-Teller effect couples the nuclear and electronic degrees of freedom of the molecule. This section discusses the role played by the Jahn-Teller effect in dynamical processes involving the H_3 molecule.

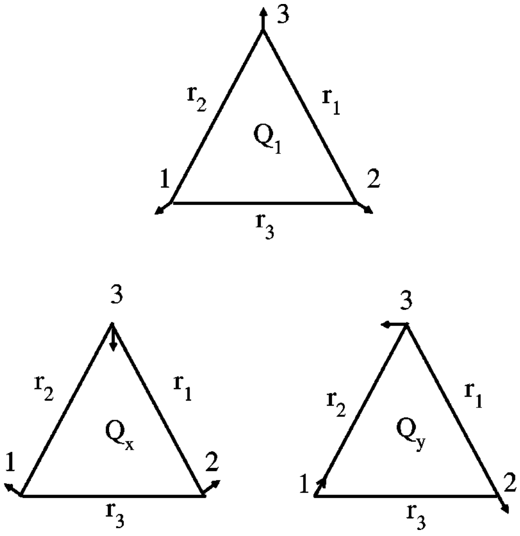

FIG. 2. Normal vibrational coordinates of the H_3^+ ion. The coordinate Q_1 (upper scheme) describes the symmetric stretch of the molecule. The lower pair Q_x and Q_y represents the doubly degenerate asymmetric stretch mode: oscillations along Q_x and Q_y have the same frequencies. An alternative doubly degenerate pair ρ, ϕ can be represented by simultaneous rotation of all six vectors shown in the two lower schemes, with ϕ being the angle of rotation (phase) and ρ being the length of the vectors (amplitude of oscillations). The motion along the angle ϕ with fixed ρ produces an effective angular momentum generated by vibration.

A. Vibrational symmetry coordinates

Apart from translations and rotations there are three vibrational degrees of freedom $\mathcal{Q}$. In this section, we use conventional vibrational symmetry coordinates $\mathcal{Q}=(Q_1,Q_x,Q_y)$ [47],

$$Q_1=f\frac{1}{\sqrt{3}}(\Delta r_1+\Delta r_2+\Delta r_3),$$

$$Q_x=f\frac{1}{\sqrt{3}}(2\Delta r_3-\Delta r_2-\Delta r_1),$$

$$Q_y=f(\Delta r_2-\Delta r_1), \qquad (15)$$

where $f=2.639\,255$ bohr^{-1} is a constant. The coordinates $\Delta r_i=r_i-r_{ref}$ describe displacements of the nuclei from the equilibrium geometry that occurs when $r_1=r_2=r_3=r_{ref}=1.6504$ bohr, r_i representing the distance between nuclei j and k (no two indices i, j, and k are equal). We introduce another set of vibrational coordinates (Q_1, ρ, and ϕ), changing the pair (Q_x, Q_y) into the pair (ρ, ϕ):

$$Q_x=\rho\cos\phi, \quad Q_y=\rho\sin\phi. \qquad (16)$$

The coordinate Q_1 describes the symmetric stretch of the molecule, whereas the pair (Q_x, Q_y) or alternatively the pair (ρ, ϕ) describe bends and the asymmetric stretch. Figure 2 indicates these three vibrational coordinates.

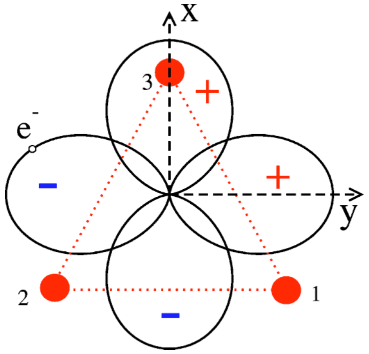

FIG. 3. The figure demonstrates the symmetry of the electronic $2p$ functions in the body frame of $H_3{}^+$. We plot the probability density of two components p_x and p_y in polar coordinates as a function of angle φ'. The third component p_z would be along the Z axis, which is perpendicular to the plane of the molecule. By plus and minus signs we specify the phase of p_x and p_y components. From the figure it is clear that the p_x and p_y components are transformed according to E representation under operations from the D_{3h} group. The p_x component (along the X axis) can be associated with an E_a function, and the p_y (along the Y axis) component is associated with an E_b function. For comparison, see the vibrational functions of the E symmetry in Fig. 7. The p_z component (not shown) transforms according to the A_1 irreducible representation. For the complete picture, one has to specify the parity of three components with respect to reflection through the XY plane. All p electronic wave functions are antisymmetric with respect to this operation, so the complete notation for the functions is E'' and A_1''. We mention also that the components p_x and p_y are related to spherical harmonics $Y_{1,1}$ and $Y_{1,-1}$ in a similar way as the vibrational functions E_a and E_b are related to $|v_2^{l_2}\rangle$ and $|v_2^{-l_2}\rangle$ states of Eqs. (25).

As was mentioned above, the ion can exist in either an A_2' or A_2'' state, while the total nuclear-spin can either be $I=3/2$ (ortho) or $I=1/2$ (para). We limit our treatment of $H_3{}^+$ DR to the p-wave component of the incident-electron wave function. In the molecular (body) frame, the electron can exist in one of the three np substates. In our treatment we choose the body-frame z axis to coincide with the symmetric-top axis. The $np\sigma$ and $np\pi$ electronic states transform according to the A_1'' and E'' irreducible representations of the $D_{3h}(M)$ permutation group. This is schematically depicted in Fig. 3. Orbital a is symmetric under the (12) permutation, and can be represented only through E_a'' eigenstates of D_{3h}, whereas orbital b is antisymmetric and is represented through E_b'' eigenstates. The orbital $p\sigma$ is not shown in the figure. It is symmetric with respect to all permutations in the xy plane, and antisymmetric under reflection through this plane, which is the σ_h operation.

B. Jahn-Teller coupling for the $np\pi$ states of H_3

According to group theory for the D_{3h} symmetry, for any principal quantum number n, two np electronic substates exist in the H_3 molecule that transform according to E'' symmetry. They have the same energy at any equilateral geometry of the three nuclei. Once this geometry is distorted, the D_{3h} symmetry is lifted and the two states are coupled. Diagonalization of the 2×2 Longuet-Higgins Hamiltonian yields two different electronic potential surfaces of H_3 that are functions of the three vibrational coordinates Q_1, ρ, and ϕ. These two surfaces are energetically degenerate only at $\rho=0$. Figure 4 shows the $2p\sigma$ and $2p\pi$ potential surfaces of H_3 as functions of the pair Q_x, Q_y (ρ,ϕ) coordinates for fixed a symmetric stretch coordinate $Q_1=0$. These potential surfaces are calculated using quantum-defect parameters from Ref. [47]. At the bottom of the figure are the potential-energy contours for the lowest state $2p\pi_l$ which has three local potential minima when the symmetric stretch coordinate Q_1 is clamped. The two highest states $2p\sigma$ and $2p\pi_2$ have only one minimum. The splitting between the two $2p\pi$ states derives from the Jahn-Teller coupling. For comparison, Fig. 5 displays the potential surfaces for $3p$ states at $Q_1=0$. Here, the three minima of the $3p\pi_l$ state are situated much closer to the point $\rho=0$. These and all higher Rydberg states of the molecule represent closed dissociation channels

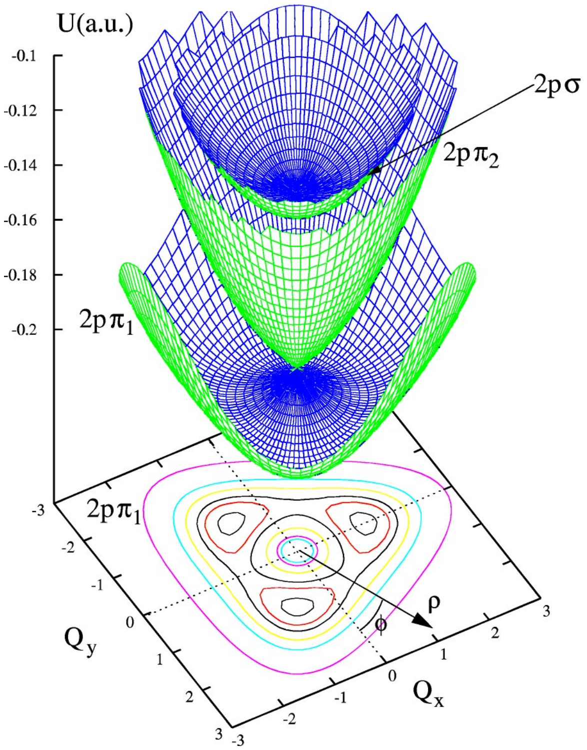

FIG. 4. The figure demonstrates how the Jahn-Teller effect produces a high rate of dissociative recombination. One $2p\sigma$ potential surface and two $2p\pi$ potential surfaces [47] of the neutral molecule are shown. The conical intersection is produced by Jahn-Teller coupling. When an electron arrives, it scatters first into a low-lying vibrationally excited Rydberg state $\{01^1\}$. Then, after the nuclei vibrate, the system finds its way with high probability into a $2p\pi$ state having high vibrational excitation, near the point of conical intersection. The contour plot at the bottom of the figure represents the lowest $2p\pi_1$ surface. All three potential surfaces are shown in the reduced 2D space of dimensionless normal coordinates. The coordinates used here are the normal asymmetric Q_x, Q_y coordinate, with ρ and ϕ their polar components [17,18]. The third vibrational coordinate—the symmetric stretch coordinate Q_1—is kept constant for this graph.

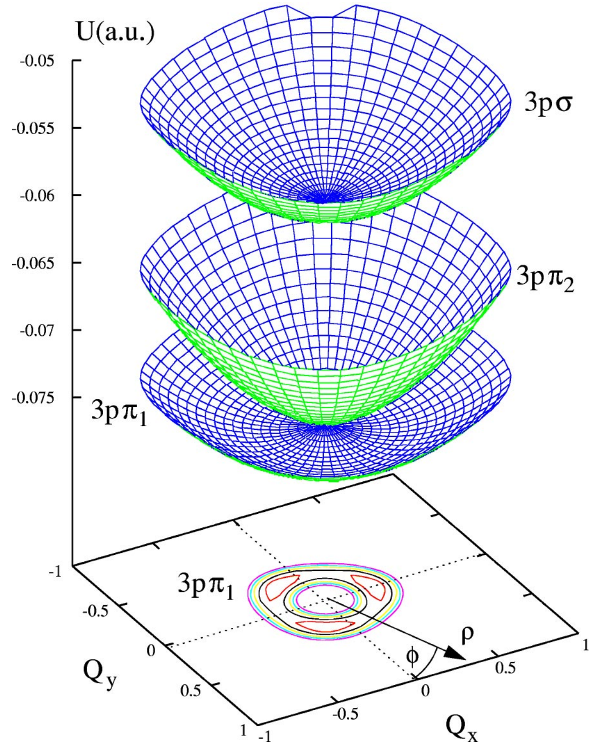

FIG. 5. Potential surfaces of $3p\pi$ and $3p\sigma$ of H_3 molecule. The dimensionless normal coordinates are the same as in Fig. 4. These and higher Rydberg np states play an important role in the process of dissociative recombination. Once the system ${H_3}^+ + e^-$ is recombined, the dissociation occurs via intermediate, mainly $np\pi$, Rydberg states, ending on the $2p\pi$ repulsive potential. Then the three-atomic molecule drives to the disintegration on H_2+H or $H+H+H$ fragments.

in the low-energy region that is our present focus. However, these play a vital indirect role as an intermediate pathway that ultimately leads to dissociative recombination. During a collision, the electron is captured into an excited Rydberg state, which is attached, most likely, to a doubly degenerate E vibrational state. Once the capture occurs, the system nonadiabatically transfers into lower Rydberg states. The descent transfers energy into the vibrational motion of the nuclei. Upon reaching the lowest Rydberg states $2p\pi$, the system dissociates.

The mechanism of such a descent was proposed and discussed previously by Schneider *et al.* [4,19]. Although these authors did not include the Jahn-Teller coupling note that this would hardly be possible in their approach of reduced dimensionality because E vibrational states cannot be properly represented. The importance of the intermediate H_3 Rydberg states for ${H_3}^+$ DR was also suggested in theoretical studies by Tashiro and Kato [20,21].

At this step of the treatment we describe the collision of an incident p-wave electron with the ion, using the collision matrix $S_{\Lambda,\Lambda'}(\mathcal{Q})$, where Λ is the body-frame projection of the electron angular momentum $l=1$. We neglect angular momenta other than that of p wave for both the incident and the scattered partial waves. Then, $S_{\Lambda,\Lambda'}(\mathcal{Q})$ represents an amplitude for the reaction

$$e^-(l=1,\Lambda')+{H_3}^+(\mathcal{Q})\rightarrow e^-(l=1,\Lambda)+{H_3}^+(\mathcal{Q}) \quad (17)$$

with the nuclei clamped. In fact, the electron scatters from one irreducible representation Λ to another Λ', while the nuclei do not have time to move. Therefore, Eq. (17) describes the short-range ${H_3}^+ + e^-$ collision in the Born-Oppenheimer approximation, where nuclear degrees of freedom are not yet coupled to the electronic degrees of freedom. The scattering matrix includes the Jahn-Teller coupling. Instead of S we use the reaction matrix $K^0_{\Lambda,\Lambda'}(\mathcal{Q})$ in the form proposed by Staib and Domcke [39]. For np states it has the form [17,18,39]

$$K^0_{\Lambda,\Lambda'}(\mathcal{Q}) = \begin{pmatrix} K_{0,0} & K_{0,1} & K_{0,-1} \\ K_{1,0} & K_{1,1} & K_{1,-1} \\ K_{-1,0} & K_{-1,1} & K_{-1,-1} \end{pmatrix} = \begin{pmatrix} \tan[\pi\mu_{\Lambda=0}(\mathcal{Q})] & 0 & 0 \\ 0 & \delta\rho^2 & \lambda\rho\exp(i\phi) \\ 0 & \lambda\rho\exp(-i\phi) & \delta\rho^2 \end{pmatrix}, \quad (18)$$

where $\mu_{\Lambda=0}$, δ, and λ are quantum-defect parameters obtained from the difference between the *ab initio* potentials of ${H_3}^+$ [48,49] and H_3 [47].

We would like to point out that the parameters δ and λ as calculated in Ref. [47], should be multiplied by factor $-\pi$ in order to be used in the present treatment. The reason is that there are two different conventions for normalizations of the K matrix (see, for example p. 2554 of Ref. [50]), differing by the factor of $-\pi$. This difference in the conventions is reflected by the values of the parameters $\mu_{\Lambda=0}$, δ, λ. Unfortunately, in Refs. [18,47], δ and λ were extracted from *ab initio* calculations implying one convention, but they were used in the K matrix as if they were in the other convention. In our previous work, Ref. [28] we have used δ and λ from Ref. [47] without realizing this incompatibility. Thus, the DR cross section estimated in Ref. [28] should be multiplied approximately by π^2 in order to account for the incompatibility.

The parameter $\mu_{\Lambda=0}$ varies slowly with $\mathcal{Q}$. The p-wave K matrix written in Eq. (18) does not include the zeroth-order phase shift $\pi\mu^0_\Lambda=\pi\mu_\Lambda(\mathcal{Q}=0)$ (where $\mu^0_{-1}=\mu^0_1$ and $\mu^0_0=0$). It can be included using the eigenvalues $\tan(\pi\tilde{\mu})=U^T K^0(\mathcal{Q})U$ of matrix (18) through the equation

$$K(\mathcal{Q})=U\tan[\pi(\tilde{\mu}+\mu^0_\Lambda)]U^T. \quad (19)$$

We use the values $\mu^0_{\pm 1}=0.395$, $\delta=-3424\ \mathrm{cm}^{-1}$, and $\lambda=-38\,830\ \mathrm{cm}^{-1}$ from Ref. [47].

The electron-ion scattering matrix for a fixed nuclear configuration $\mathcal{Q}$ can be written in terms of the diagonal matrix of eigenphase shifts $\pi\tilde{\mu}$ using

$$S(\mathcal{Q})=Ue^{2\pi i(\tilde{\mu}+\mu^0_\Lambda)}U^T, \quad (20)$$

where the matrix indices specify different possible projections Λ of the electron angular momentum l onto the symmetric-top axis (z axis) of the ion.

Since the parameters of the K matrix of Eq. (18) have been fitted to *ab initio* potential surfaces of H_3 and H_3^+, information about potentials of np states of H_3 has been incorporated into our quantum-defect description, and they can be represented within the Born-Oppenheimer approximation by

$$U_n^{\Lambda}(\mathcal{Q})=U^{+}(\mathcal{Q})-\frac{1}{2\nu_{n,\Lambda}^2}. \qquad (21)$$

Here, the index Λ distinguishes between a $p\sigma$ state or one of the two $p\pi$ states. The effective quantum number is given by $\nu_{n,\sigma}=n-\mu_{\Lambda=0}$. The effective quantum numbers $\nu_{n,\pi_{1,2}}$ of the $np\pi$ states are calculated by diagonalizing the matrix of Eq. (18). This gives

$$\nu_{n,\pi_{1,2}}(\mathcal{Q})=n-\pi^{-1}\arctan(\delta\rho^2\mp\lambda\rho)-\mu_e^0, \qquad (22)$$

where the integer n is the principal quantum number. Equations (21) and (22) can be used to calculate the Born-Oppenheimer potential surfaces given in Figs. 5 and 4. This calculation adopts the *ab initio* H_3^+ ionic potential surface given in Refs. [48,49].

IV. TREATMENT OF H_3^+ VIBRATIONAL DYNAMICS USING AN ADIABATIC HYPERSPHERICAL APPROACH

To treat the vibrational dynamics in three dimensions, we employ the adiabatic hyperspherical approach. Although this method has been described several times (e.g., Refs. [23,33,34]), a number of alternative definitions exist for the hyperspherical coordinates. For the sake of brevity, we limit the present discussion to the actual formulas utilized.

A. Hyperspherical coordinates

Keeping aside overall rotations and translations of the system, only three internuclear distance coordinates $\mathcal{Q}\equiv\{r_1,r_2,r_3\}$ are needed to describe the nuclear positions. In this notation, for instance, r_1 is the distance between nuclei 2 and 3. We express $\mathcal{Q}$ in terms of three coordinates, a hyperradius R and two hyperangles θ and φ, which are defined here by

$$r_1=3^{-1/4}R\sqrt{1+\sin\theta\sin\left(\varphi+\frac{2\pi}{3}\right)},$$

$$r_2=3^{-1/4}R\sqrt{1+\sin\theta\sin\left(\varphi-\frac{2\pi}{3}\right)},$$

$$r_3=3^{-1/4}R\sqrt{1+\sin\theta\sin\varphi}. \qquad (23)$$

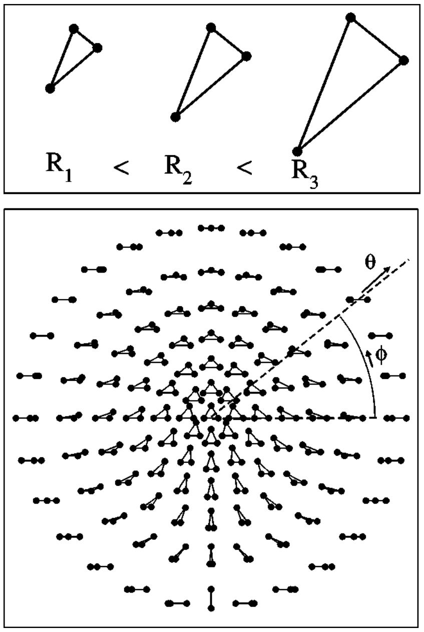

FIG. 6. Hyperspherical coordinates for three particles. All possible configurations of the three particles can be described by a hyper-radius $R\in[0,\infty)$ and two hyperangles $\theta\in[0,\pi/2]$ and $\phi\in[0,2\pi)$. The upper panel shows three configurations for three different values of the hyper-radius; both hyperangles are fixed. The hyper-radius describes the size of the system, but it says nothing about the shape of the three-particle triangle. The shape of the system is described by the two hyperangles. The lower panel gives all possible configurations of the three-particle triangle for all values of the hyperangles. The angle ϕ is cyclic, θ is not. All particle permutations are represented by a change in the angle ϕ. Three two-particle permutations (12), (23), and (13) correspond to reflections with respect to axes $\phi=-\pi/2$, $\phi=\pi/6$, and $\phi=5\pi/6$. The effect of operations (123) and (132) corresponds to a change of the angle ϕ on $\phi\pm2\pi/3$. Thus, the hyperspherical angles are well adapted to symmetry properties for a description of the H_3^+ vibrational motion.

In these formulas the hyperangle θ ranges from 0 to $\pi/2$, while the hyperangle φ ranges from 0 to 2π, and the hyperradius R extends from 0 to ∞.

The two hyperangles and the hyperradius are equivalent to the set of three internuclear distances (r_1,r_2,r_3). The hyper-radius can be viewed qualitatively as the "size coordinate" of the system. At fixed values of the two hyperangles, an increase of the hyperradius expands the size of the system without changing its shape, as is shown in the upper panel of Fig. 6. In contrast, changing the hyperangles at a fixed value of the hyperradius sweeps the system through all possible shapes without changing its overall size. The possible shapes of the triangle formed by the nuclei are shown in the lower panel of Fig. 6, which resembles a Dalitz plot, Ref. [51].

A solution of the vibrational Schrödinger equation with an appropriate interaction potential in the three-dimensional hyperspherical space is equivalent to the solution in the space of (r_1,r_2,r_3). Instead of this, we fix the hyperradius R and solve the Schrödinger equation in the space of two hyperangles θ and φ,

$$H_R\Phi_i(\theta,\phi;R)=U_i^+(R)\Phi_i(\theta,\phi;R),$$

$$H_R=\frac{\Lambda^2}{2\mu R^2}+\frac{15}{8\mu R^2}+V(R,\theta,\varphi). \tag{24}$$

In this equation, Λ^2 is the squared "grand angular momentum" operator [24] and $\mu=m/\sqrt{3}$ is the three-body reduced mass of the system, m being the atomic hydrogen mass. $V(R,\theta,\varphi)$ is the molecular potential; in this case it is the ionic potential surface of H_3^+ [48,49].

We call the resulting eigenfunctions $\Phi_i(\theta,\phi;R)$ adiabatic hyperspherical states and the eigenvalues $U_i^+(R)$ the adiabatic hyperspherical potential curves. They depend parametrically on the hyperradius. After the calculation is performed at many different values of the hyperradius, we obtain a set of hyperspherical potential curves $U_i^+(R)$. The lowest ionic hyperspherical curve is shown in Fig. 1. The first 200 $J=0$ H_3^+ hyperspherical curves are displayed in Ref. [28].

B. Classification of vibrational wave functions

In the reduced two-dimensional space of hyperangles, $\{\theta,\phi\}$, each C_{3v} symmetry group element is represented by a corresponding transformation of hyperangles. The hyperradius does not influence any C_{3v} operation. The vibrational channel functions $\Phi_i(\theta,\phi)$—hyperspherical states—can thus be classified according to irreducible representations of the group C_{3v}, namely, A_1, A_2, or E. The representation E is two dimensional, whereby it has two degenerate states E_a and E_b, which can be transformed into linear combinations of each other through group symmetry operations. To distinguish between the two E states consistently, we choose E_a to be symmetric under the (12) operation and E_b to be antisymmetric. This choice of E_a and E_b wave functions follows from Ref. [52]. When the actual vibrational Hamiltonian is numerically diagonalized in the two-dimensional space of the hyperangles θ and ϕ, the resulting two degenerate wave functions of E symmetry typically turn out to be mixed, giving in essence combinations $E_{1,2}=E_a\cos\alpha\pm E_b\sin\alpha$. In order to recast them as the well-defined pair E_a,E_b, we construct the matrix P^{12} of the permutation operation (12) in the basis of the two states $E_{1,2}$ and diagonalize it. The eigenstate having the eigenvalue $+1$ is the E_a state and the eigenstate with the eigenvalue -1 is the E_b state.

Figure 7 shows the first several $\Phi_i(\theta,\phi)$ eigenstates having different symmetries for a fixed hyper-radius of $R=2.2$ bohr. The wave functions are shown as contour plots in a polar representation of the two hyperangles. The "azimuthal angle" in this representation is ϕ, while the "polar radius" in this hyperangle space is taken to be θ. The corresponding configurations of the nuclei are identified on Fig. 6.

All eigenstates $\Phi_i(\theta,\phi)$ and corresponding adiabatic potential curves $U_i^+(R)$ are thus classified according to one of the irreducible representations A_1, A_2, E_a, or E_b. Potential curves $U_i^+(R)$ associated with different irreducible representations can cross, whereas potential curves of the same symmetry do not cross.

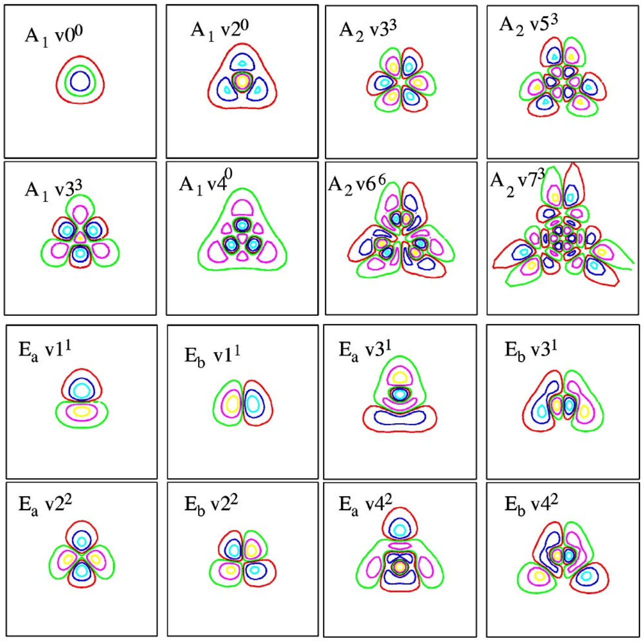

FIG. 7. The figure gives several adiabatic vibrational wave functions of H_3^+, calculated for a fixed hyperradius $R=2.2$. The wave functions are represented with contour plots as functions of the two hyperangles. The connection between the contour plots and actual configurations of the three nuclei is given in the lower panel in Fig. 6. Every contour plot is labeled with a corresponding symmetry and with a triad of vibrational quantum number $\{v_1,v_2^{l_2}\}$. The quantum number v_1 is not specified. It is linked to the number of symmetric stretch quanta. In the adiabatic approximation, the number of symmetric stretch quanta is associated with motion along the hyperradius.

The vibrational states of H_3 are labeled by the familiar triad $\{v_1,v_2^{l_2}\}$, where v_1 describes the symmetric stretch vibrational quantum number and the $v_2^{l_2}$ pair describes two asymmetric modes (v_2 the quantum of the asymmetric stretch mode and l_2 the vibrational angular momentum). In the adiabatic hyperspherical approximation, which neglects the coupling between different $U_i^+(R)$ states having the same symmetry, the quantum of excitation in the hyperradius is the v_1 quantum number, while the quanta in the two hyperangles are described by $v_2^{l_2}$. The index i labeling $\Phi_i(\theta,\phi)$ can therefore be recast as $v_2^{l_2}$. Figure 7 gives the quantum numbers of these hyperspherical eigenfunctions.

In order for all vibrational states to transform uniformly according to Table III some additional transformations of the obtained real vibrational wave functions should be performed. The E_b and E_a states, constructed in the way described above, transform accordingly under the (12) operation, but the mutual phase of these states has not yet been specified. This phase is important for the construction of properly symmetrized rovibrational ionic eigenstates. An appropriate, consistent choice of phase is adopted through the following procedure. We have found that our treatment is the simplest if we define an alternative linear combination of the two degenerate E states,

TABLE V. Accuracy test of the adiabatic hyperspherical approach: a comparison between several vibrational energies calculated in the present approach and those from a full three-dimensional diagonalization [49].

Symmetry	$v_1, v_2^{l_2}$	Adiabatic approximation (cm^{-1})	Jaquet *et al.* [49] (cm^{-1})
A_1	00^0	0	0
A_1	10^0	3188	3178.15
E	01^1	2516	2521.20
E	11^1	5554	5553.94
E	02^2	5001	4997.73
E	12^2	7896	7869.82
E	03^1	6978	7005.81
A_2	03^3	7482	7491.89
A_2	13^1	10 243	10 209.55

$$|v_2^{l_2}\rangle = \frac{1}{\sqrt{2}}(E_a + iE_b),$$

$$|v_2^{-l_2}\rangle = \frac{1}{\sqrt{2}}(E_a - iE_b), \tag{25}$$

where we assume that $l_2 > 0$. The operation (123) transforms the $|v_2^{\pm l_2}\rangle$ wave functions as $(123)|v_2^{\pm l_2}\rangle = e^{(s2\pi i l_2/3)}|v_2^{\pm l_2}\rangle$, where $s=1$ or -1. If we keep the E_a state fixed, E_b should be multiplied by 1 or -1 to obtain the following transformations:

$$(123)|v_2^{\pm l_2}\rangle = e^{(\pm 2\pi i l_2/3)}|v_2^{\pm l_2}\rangle, \quad l_2 > 0, \tag{26}$$

in agreement with Table III. Finally, we multiply all vibrational functions A_2 by i in order to obtain a real reaction matrix K when outgoing-wave hyper-radial channel functions are real. (In fact, owing to our use of outgoing-wave hyper-radial Siegert states, our reaction matrix turns out to be complex but symmetric.)

C. Accuracy of the adiabatic hyperspherical approximation for H_3^+

After the adiabatic hyperspherical potential curves $U_i^+(R)$ are determined, we calculate vibrational energies $E_{i,v}$ by solving the adiabatic hyperradial equation

$$\left(-\frac{1}{2\mu}\frac{\partial^2}{\partial R^2} + U_i^+(R)\right)\psi_{i,v}^+(R) = E_{i,v}\psi_{i,v}^+(R). \tag{27}$$

Here $\{i,v\} \equiv \{v_1, v_2^{l_2}\}$. Table V compares the resulting vibrational energies determined by a full three-dimensional diagonalization [49] with those obtained in the adiabatic hyperspherical approximation.

V. SIEGERT PSEUDOSTATE DESCRIPTION OF ESCAPING DISSOCIATIVE FLUX

In this section, we discuss the issues involved in our description of the dissociation of the neutral molecule H_3. For brevity, we omit rotational quantum numbers since the rotational degrees of freedom play no role in this aspect of the theory.

The initial ionic state of H_3^+ in dissociative recombination experiments is the ground $\{00^0\}$ vibrational state; it is bound. Once the electron is captured by the ion, the system can dissociate, since the relevant H_3 potentials are repulsive. The fact that the system is characterized by attractive ground-state ionic potential curves but repulsive $2p\pi$ H_3 curves is evident from Fig. 1. However, the dissociation proceeds through a number of excited Rydberg states, which are bound with respect to dissociation. While the system is in one of the excited Rydberg states, autoionization is a competing mechanism, especially in the region of configuration space where the three atoms are close to each other. Usually, multichannel quantum-defect theory treats such a system as a set of coupled vibrational states: each potential curve (ionic and neutral) generates a certain number of vibrational levels. These ionic and neutral vibrational states have to be taken into account. The interaction between them are determined in an appropriate way [7]. In order to describe the process of dissociation, the vibrational continuum of all or certain potential curves should be somehow introduced into the model. It can be done, for example, through discretization of the continuum [11,53] for all necessary potential curves. Although this procedure can be applied in our case it requires a lot amount of calculations, since the MQDT calculation must be carried out for many different values of the hyper-radius.

Recently, an alternative to this discretization method was presented [29], which utilizes the recently developed Siegert pseudostate's formulation [54,55]. The Siegert pseudostates at low energies, which correspond to the ordinary discrete spectrum of each hyperspherical potential curve, coincide to machine precision with the ordinary bound-state vibrational wave functions. In contrast, the vibrational continuum is described by Siegert pseudostates that obey outgoing-wave boundary conditions at the outermost surface. The number of Siegert pseudostates taken into account in our treatment is limited by the energy of the highest vibrational level that can contribute to the final DR cross section. For a limited box size, the vibrational spectrum is discrete. Thus, the total number of vibrational states in our treatment is finite, although we include vibrational states belonging to the dissociative continuum. These Siegert vibrational pseudostates are introduced in order to permit the dissociative flux to escape when it reaches the boundary. In familiar techniques using a box discretized continuum obeying Dirichlet boundary conditions, this flux is reflected by the boundary artificially. Every bound and Siegert pseudostate of every ionic potential curve generates a Rydberg series of neutral states. The outgoing-wave boundary conditions enforced for the ionic Siegert pseudostates simulate the absorption of the dissociative flux of the neutral molecule. The next step of the treatment is the construction of the scattering matrix describing the collision of an electron with the ion. The set of ionic channels is the set of all bound and Siegert pseudostates calculated for every ionic potential curve. The presence of Siegert pseudostates simulates the possibility for the system to escape from this ionic subspace, which makes the scattering matrix nonunitary. In fact, the physically-relevant columns of the S matrix are subunitary in the sense that the sum of squares of the elements of each such column is *less* than unity. Moreover, the associated difference from unitarity measures the probability of dissociative recombination. The following section describes the quantitative implementation of this procedure.

A. Siegert pseudostates in the hyperradius

In our treatment, every hyperspherical potential curve $U_i^+(R)$ possesses its own distinct set of vibrational Siegert pseudostates, which are determined separately for each curve using the linearization procedure described by Tolstikhin *et al.* [54,55]. These states satisfy the adiabatic hyperspherical Schrödinger equation (27), with outgoing-wave boundary conditions at some large but finite hyperradius R_f:

$$\left(\frac{d}{dR}-ik_{i,v}\right)\psi_{i,v}(R)|_{R=R_f}=0. \tag{28}$$

We normalize the Siegert pseudostates so that they obey the following orthonormality condition:

$$\int_0^{R_f}\psi_{i,v}(R)\psi_{i,v'}(R)dR+i\,\frac{\psi_{i,v}(R_f)\psi_{i,v'}(R_f)}{k_{i,v}+k_{i,v'}}=\delta_{vv'}. \tag{29}$$

In our treatment, for searching the Siegert pseudostates we implement the linearization procedure proposed by Tolstikhin *et al.* [54,55]. We adopt basis splines as our representation basis. Nonorthogonality of the basis splines requires some simple modification of the linear eigensystem, as has been discussed elsewhere [29]. The wave numbers $k_{i,v}^2$ and energies $E_{i,v}$ are linked by $E_{i,v}=k_{i,v}^2/(2\mu)+D_i$, where D_i is evaluated at the outer boundary of the hyperradius, $D_i=U_i^+(R_f)$.

For energies $E_{i,v}=k_{i,v}^2/(2\mu)+D_i$ below the corresponding dissociation limit D_i, the Siegert pseudostates are equivalent to the ordinary bound vibrational states. The spectrum of the linearization procedure of Refs. [54,55] is obtained from the complex momentum space $k_{i,v}$, while the complex $k_{i,v}$ always occur in the spectrum in pairs: if $\mathrm{Re}(k_{i,v})>0$ and if $k_{i,v}$ is in the spectrum, $-k_{i,v}^*$ is also in the spectrum. In the energy domain, it implies that bound states are present twice in the spectrum. Namely, if the real part of $k_{i,v}$ is zero (a bound state), both $k_{i,v}$ and $-k_{i,v}$ present in the spectrum giving the same energy $E_{i,v}=k_{i,v}^2/(2\mu)+D_i$. The wave functions of the pair of conjugated states are different. In our treatment we need one state from the pair. From the pair of conjugated states $E_{i,v}$, and $E_{i,v}^*$ we keep only the state with a negative imaginary part, which corresponds to a decaying state. This choice implies that the real part of the wave number $k_{i,v}$ is positive (outgoing wave).

B. Details of numerical calculation

In the present calculations of the DR rate, for every set of quantum numbers $\{I,\Gamma,N^+,N\}$, describing the total symmetry of the ${H_3}^++E^-$ system, typically we used 50–100 hyperspherical potential curves and 8–12 Siegert vibrational states. The grid in hyper-radius is taken from 1 a.u. to 4.5 a.u. with 64 mesh points. The accuracy of the present calculation is influenced only by the number of hyperspherical states and Siegert states taken into account. Trial calculations carried out with larger numbers of hyperspherical (150) and vibrational (20) states for certain values of $\{I,\Gamma,N^+,N\}$ suggest that the convergence error of the final rate varies with the electron energy but does not exceed 20%. Due to its smooth character, the thermally averaged DR rate is much less sensitive to the total number of included states, especially at higher temperatures. The total number of different sets $\{I,\Gamma,N^+,N\}$ taken into account in the present treatment is 17. The most time-consuming part of the calculation is the repeated solution of the usual channel-elimination formula of MQDT [see Eq. (44) below], which involves solution of an inhomogeneous linear system of equations of dimension up to 2000×2000, at ≈100 000 energy mesh points, for every set of quantum numbers. This requires ≈10 000 CPU hours, but far less real time because the calculation is carried out in parallel.

C. Vibrational-frame transformation using the adiabatic hyperspherical method with Siegert pseudostates

Once the Siegert pseudostates are calculated, the scattering matrix describing the collision of the electron with the vibrating ${H_3}^+$ ion can be constructed. The theory of the vibrational frame transformation [11] can be used to calculate the transition amplitude $S_{i,i'}$ from one vibrational state to another. In the present treatment, the composite channel indexes i and i' specify both the ionic vibrational state and the electron orbital momentum projection Λ. The vibrational index is the triad of quantum numbers, $v_1,v_2^{l_2}$. Since we have employed the hyperspherical adiabatic approximation, every pair $v_2^{l_2}$ determines a hyperspherical curve $U_i^+(R)$, and the index v_1 labels the different Siegert pseudostates that lie within that curve. Therefore, the amplitude $S_{i,i'}$ for the process

$$e^-(\Lambda')+{H_3}^+(v_1',{v_2'}^{l_2'})\rightarrow e^-(\Lambda)+{H_3}^+(v_1,v_2^{l_2}) \tag{30}$$

is calculated in two steps, which parallels the two-step calculation of vibrational energies:

$$S_{v_2,l_2,\Lambda;v_2',l_2',\Lambda'}(R)=\langle\langle\Phi_{v_2,l_2}|S_{\Lambda;\Lambda'}(\mathcal{Q})|\Phi_{v_2',l_2'}\rangle\rangle^{(R)}. \tag{31}$$

Here, the double brackets imply an integration over the hyperangles at a fixed value R of the hyper-radius. The scattering matrix $S(\mathcal{Q})$ as a function of nuclear geometry $\mathcal{Q}$ was introduced in Eq. (20). Similarly, the second step of the frame transformation reads

$$S_{v_1,v_2,l_2,\Lambda;v_1',v_2',l_2',\Lambda'} = \langle \psi_{v_1,v_2,l_2}(R)|S_{v_2,l_2,\Lambda;v_2',l_2',\Lambda'}(R)|\psi_{v_1',v_2',l_2'}(R)\rangle_S . \tag{32}$$

In this notation, the brackets $\langle\ \rangle_S$ are meant to imply a volume integration in the sense of Siegert pseudostates, i.e., with the usual additional surface term [29]:

$$\langle \psi_{v_1,v_2,l_2}(R)|S_{v_2,l_2,\Lambda;v_2',l_2',\Lambda'}(R)|\psi_{v_1',v_2',l_2'}(R)\rangle_S = \int_0^{R_f} \psi_{v_1,v_2,l_2}(R) S_{v_2,l_2,\Lambda;v_2',l_2',\Lambda'}(R)\psi_{v_1',v_2',l_2'}(R)dR + i\,\frac{\psi_{v_1,v_2,l_2}(R_f)S_{v_2,l_2,\Lambda;v_2',l_2',\Lambda'}(R_f)\psi_{v_1',v_2',l_2'}(R_f)}{k_{v_1,v_2,l_2}+k_{v_1',v_2',l_2'}} . \tag{33}$$

Note that one omits the usual complex conjugation of the bra wave function $\psi_{v_1,v_2,l_2}(R)$. This is in parallel with the Siegert state normalization relation of Eq. (29). Owing to the presence of Siegert states with complex eigenenergies, this electron-ion scattering matrix is not unitary (implying that the corresponding reaction matrix is not Hermitian). The nonunitarity accounts for the fact that the electron can become stuck in the ion, resulting in dissociation of the system into neutral products.

VI. ROTATIONAL- AND VIBRATIONAL-FRAME TRANSFORMATIONS FOR AN ELECTRON COLLIDING WITH H$_3^+$

The electron-ion scattering matrix constructed in the preceding section does not yet incorporate the possibility of different ionic rotational excitations. If the H$_3^+$ ion is initially in one rotational state $(N^{+\prime},K^{+\prime})$, the collision with the electron can change its rotational state to (N^+,K^+). The elements $\mathcal{S}_{i,i'}$ of the total scattering matrix $\mathcal{S}$ thus should describe the transition amplitude to change from one rovibrational state $i'=\{v_1',v_2'^{l_2'}\}(N^{+\prime},K^{+\prime})$ to another $i=\{v_1,v_2^{l_2}\}(N^+,K^+)$. As a notational convention, we do not include in the indexes i and i' the quantum numbers that are conserved during the collision.

The change in the rotational excitation $(N^{+\prime},K^{+\prime})\rightarrow(N^+,K^+)$ can be treated accurately using the rotational-frame-transformation approximation [11]: these transitions occur primarily when the electron Rydberg period is comparable to the ionic rotational period. The qualitative idea implemented here is the same as was introduced by Fano [40]. The initial rotational channel function is projected onto short-range rotational states specified by two quantum numbers: the projection Λ of the electron orbital momentum $\vec{l}$ onto the symmetric-top axis and the projection K of the total angular momentum $\vec{N}=\vec{N}^+ + \vec{l}$ onto the same axis. N and l are conserved quantum numbers in both the long- and short-range rotational representations. Below, we give a detailed description of the rovibrational frame transformation for the $e^- + \mathrm{H}_3^+$ system, specifying all quantum numbers in both regions of interaction.

A. Construction of wave functions for the $e^- + \mathrm{H}_3^+$ system

At large distances between the electron and ion, the system is described by the electron orbital angular momentum l and its projection λ on the laboratory z-axis, by the total ionic angular momentum N^+, its projection m^+ on the laboratory z-axis and its projection K^+ on the body-fixed axis Z. Z is chosen to coincide with the C_3 molecular axis. Correspondingly, we represent the wave function of the $e^- + \mathrm{H}_3^+$ system by the product of the ionic $\Phi_t^{n.sym}$ and electronic $Y_{l\lambda}(\theta,\varphi)$ wave functions,

$$\mathcal{R}(N^+,m^+,K^+;\alpha\beta\gamma)Y_{l\lambda}(\theta,\varphi)\mathcal{V}(v_1,v_2^{l_2})\Phi_I . \tag{34}$$

The angles θ,φ are spherical angles of the electron in the laboratory system (LS).

At short distances, the most appropriate molecular states are the states that approximately diagonalize the Hamiltonian. These states are specified by the projection Λ of the electron momentum on the molecular Z axis, three internuclear coordinates $\mathcal{Q}$, total angular momentum l of the system N, including the electron momentum; by the projection K of the total momentum N on Z; and by the projection of N on the laboratory z axis, m. Thus, the total wave function at short distances can be represented as

$$\mathcal{R}(N,m,K;\alpha\beta\gamma)Y_{l\Lambda}(\theta',\varphi')|\mathcal{Q}\rangle\Phi_I . \tag{35}$$

Angles θ' and φ' determine the position of the electron with respect to the molecular system (MS). Having identified the short- and long-distance states, we need to find the transformation between them. Using the transformation

$$Y_{l\lambda}(\theta,\varphi)=\sum_\Lambda Y_{l\Lambda}(\theta',\varphi')D^1_{\Lambda,\lambda}(-\gamma,-\beta,-\alpha) = \sum_\Lambda Y_{l\Lambda}(\theta',\varphi')[D^1_{\lambda,\Lambda}(\alpha\beta\gamma)]^* \tag{36}$$

between short- and long-range electronic wave functions and the expansion of the product of two Wigner functions:

$$D^{N^+}_{m^+,K^+}(\alpha\beta\gamma)D^1_{\lambda,\Lambda}(\alpha\beta\gamma) = \sum_N D^N_{m,K}(\alpha\beta\gamma)C^{N,K}_{N^+,K^+;l,\Lambda}C^{N,m}_{N^+,m^+;l,\lambda} , \tag{37}$$

the wave function of Eq. (34) is written as

$$
\begin{aligned}
&\mathcal{R}(N^{+},m^{+},K^{+};\alpha\beta\gamma)Y_{l\lambda}(\theta,\varphi)\mathcal{V}(v_1,v_2^{l_2})\\
&\quad=\left[\frac{2N^{+}+1}{8\pi^2}\right]^{1/2}\sum_{\Lambda}\,[D^{N^{+}}_{m^{+},K^{+}}(\alpha\beta\gamma)]^{*}[D^{1}_{\lambda,\Lambda}(\alpha\beta\gamma)]^{*}\\
&\qquad\times Y_{l\Lambda}(\theta',\varphi')\mathcal{V}(v_1,v_2^{l_2};\mathcal{Q})\\
&\quad=\left[\frac{2N^{+}+1}{8\pi^2}\right]^{1/2}\sum_{\Lambda}\,\sum_{N}\,[D^{N}_{m,K}(\alpha\beta\gamma)]^{*}C^{N,K}_{N^{+},K^{+};l,\Lambda}\\
&\qquad\times C^{N,m}_{N^{+},m^{+};l,\lambda}Y_{l\Lambda}(\theta',\varphi')\mathcal{V}(v_1,v_2^{l_2};\mathcal{Q})\\
&\quad=\sum_{\Lambda}\,\sum_{N}\left[\frac{2N^{+}+1}{2N+1}\right]^{1/2}C^{N,K}_{N^{+},K^{+};l,\Lambda}C^{N,m}_{N^{+},m^{+};l,\lambda}\\
&\qquad\times\mathcal{R}(N,m,K;\alpha\beta\gamma)Y_{l\Lambda}(\theta',\varphi')\mathcal{V}(v_1,v_2^{l_2};\mathcal{Q})\\
&\quad=\sum_{\Lambda}\,\sum_{N}\,C^{N^{+},K^{+}}_{l,-\Lambda;N,K}(-1)^{1-\Lambda}C^{N,m}_{N^{+},m^{+};l,\lambda}\\
&\qquad\times\mathcal{R}(N,m,K;\alpha\beta\gamma)Y_{l\Lambda}(\theta',\varphi')\mathcal{V}(v_1,v_2^{l_2};\mathcal{Q}).
\end{aligned}
\tag{38}
$$

We omitted the factor Φ_I which remains unchanged at every step of the transformation.

Short-range states have a definite total angular momentum *N*. We want to construct the long-range states having a definite total angular momentum *N*, too. In order to achieve this goal, we form the following linear combinations of the states of Eq. (38):

$$
\begin{aligned}
&|N^{+},K^{+};N,m;v_1,v_2^{l_2}\rangle\\
&\quad=\sum_{\lambda}\,C^{N,m}_{N^{+},m^{+};l,\lambda}\mathcal{R}(N^{+},m^{+},K^{+};\alpha\beta\gamma)\\
&\qquad\times Y_{l\lambda}(\theta,\varphi)\mathcal{V}(v_1,v_2^{l_2})\Phi_I.
\end{aligned}
\tag{39}
$$

We also redefine the short-range states introducing an additional factor $(-1)^{1-\Lambda}$:

$$
\begin{aligned}
|N,K,m,\Lambda;v_1,v_2^{l_2}\rangle&=(-1)^{1-\Lambda}\mathcal{R}(N,m,K;\alpha\beta\gamma)\\
&\quad\times Y_{l\Lambda}(\theta',\varphi')|\mathcal{Q}\rangle\Phi_I.
\end{aligned}
\tag{40}
$$

After these new definitions of the short- and long-range states, the transformation between them becomes very simple:

$$
|N^{+},K^{+};N,m;v_1,v_2^{l_2}\rangle=\sum_{\Lambda}\,C^{N^{+},K^{+}}_{l,-\Lambda;N,K}|N,K,m,\Lambda;v_1,v_2^{l_2}\rangle,
\tag{41}
$$

which can be considered as if two angular momenta $\vec{N}$ and $\vec{l}$ with projections K and $-\Lambda$ are added to give the angular momentum $\vec{N}^{+}$ with the projection $K^{+}=K-\Lambda$. Quantum numbers $N,l,m;v_1,v_2^{l_2}$ are not changed by the transformation of Eq. (41). They are good quantum numbers in both representations.

Note that in Eq. (41) all the projections Λ,K,K^{+},m of angular momenta can be negative or positive. It is different, for example, from Ref. [56] where all rotational functions are symmetrized with respect to different signs of projections. At this stage of the treatment, we keep both negative and positive projections explicitly in order to symmetrize products of rotational, vibrational, and nuclear-spin components simultaneously with respect to all three sets of quantum numbers. This greatly simplifies all the formulas, because it avoids, for example, the somewhat complicated symmetrization procedures of the type given by Spirko *et al.* in Ref. [52] [see Eqs. (59)–(77) of Ref. [52]].

B. Construction of the $e^{-}+\mathrm{H}_3^{+}$ scattering matrix

Now the total laboratory-frame scattering matrix can be constructed using the techniques of the frame transformation: when the electron is far from the ion, the long-range wave function diagonalizes the interaction Hamiltonian; at short distances, short-range wave functions almost diagonalize the Hamiltonian. The short-range Hamiltonian is not exactly diagonal in the basis of states of Eq. (35). It has off-diagonal elements with respect to Λ owing to the Jahn-Teller coupling. The following selection rules can be formulated: (i) the Hamiltonian only couples vibrational states of the same vibrational symmetry and the same value of Λ or (ii) it can couple the rovibrational channels according to the rule $(\Lambda=1,l_2=-1)\leftrightarrow(\Lambda'=-1,l_2'=1)$. These selection rules ensure that the parity of the system and the quantum number *G* related to the total rovibrational angular momentum are conserved during the collision.

The scattering matrix $S_{\Lambda,\Lambda'}(\mathcal{Q})$ including the Jahn-Teller coupling is given by Eqs. (18) and (20) in the basis of short-range channel functions. In the basis of rovibrational molecular states of Eq. (41), the scattering matrix $\mathcal{S}$ is

$$
\mathcal{S}^{(N,K,m,l,G)}_{N^{+},K^{+},v_1,v_2^{l_2};N^{+\prime},K^{+\prime},v_1',v_2'^{l_2'}}=\sum_{\Lambda,\Lambda'}\,C^{N^{+\prime},K^{+\prime}}_{l,-\Lambda';N,K}\left[\int_s\mathcal{V}(v_1',v_2'^{l_2'};\mathcal{Q})S_{\Lambda,\Lambda'}(\mathcal{Q})\mathcal{V}(v_1,v_2^{l_2};\mathcal{Q})d\mathcal{Q}\right]C^{N^{+},K^{+}}_{l,-\Lambda;N,K}.
\tag{42}
$$

The integral $\int_s$ in the above equation is the usual integral over vibrational coordinates if one of both the vibrational functions are bound. If both are unbound, the integral has an additional term describing the possibility for the vibrational flux to escape from the interaction zone [29]. See the discussion above. The scattering matrix of Eq. (42) is diagonal in the quantum numbers *N*, *K*, *l*, *G*, and *m*. Therefore, the cross section can be calculated separately for all combina-

TABLE VI. Probabilities of rotational excitation of the ion, induced by a colllision with a low electron.

Symmetry, I N	A_2',3/2 2	A_2',3/2 4	A_2'',1/2 1	A_2'',1/2 2	A_2'',1/2 2	A_2'',1/2 2
$(N^{+\prime},K^{+\prime})\rightarrow(N^+,K^+)$	(1,0)→(3,0)	(3,0)→(5,0)	(1,1)→(2,1)	(1,1)→(2,1)	(1,1)→(3,1)	(2,1)→(3,1)
Probability	0.74	0.76	0.79	0.15	0.5	0.27

tions of these numbers. The total scattering matrix of Eq. (42) is calculated using nonsymmetrized states of the type of Eqs. (4) and (39). Only at this stage do we carry out the symmetrization procedure described by Eq. (13). The symmetrization procedure is performed directly on the scattering matrix.

Let the total dimension of the $\mathcal{S}_{N^+,K^+,v_1,v_2^{l_2};N^{+\prime},K^{+\prime},v_1',v_2'^{l_2'}}$ matrix be $N_{tot}\times N_{tot}$. What is not specified explicitly is the total molecular symmetry $\Gamma=A_2'$ or A_2'' of the considering state and the total spin $I=1/2$ or 3/2. These quantum numbers are also conserved during a collision. For the full specification of the scattering process, ionization energies of rovibrational states $i=\{v_1,v_2^{l_2}\}(N^+,K^+)$; $i=1,2,\ldots,N_{tot}$ should be specified. We use very accurate energies available in the literature [57–60]. For some excited rovibrational levels, where no data exists, the energies were calculated using adiabatic hyperspherical and rigid-rotor approximations.

Equation (42) gives the $N_{tot}\times N_{tot}$ scattering matrix describing collisions of an electron with a vibrating and rotating ion. The matrix also contains information about the probability of dissociation of the neutral molecule formed during the collision process. Accordingly, this matrix is used for analyzing the dissociative recombination. This matrix can be also used to interpret photoabsorption experiments with the H_3 molecule [47,61]. This application will be discussed in a separate paper.

C. Probability of rotational excitation of the ion by electron impact

We will show below how the initial rotational excitation of a molecular ion can sometimes play a key role in dissociative recombination. Moreover, not every electron-ion collision leads to dissociation; in a storage ring or other environments, nondissociative collisions can sometimes change the ionic quantum state. Therefore, it is important to understand whether or not hot electrons can heat the ${H_3}^+$ rotational and vibrational degrees of freedom. Vibrational energy splittings are much larger than rotational splittings, with the first excited vibrational level $\{01^1\}$ being 0.3 eV above the ground vibrational level $\{00^0\}$. For this reason, we only discuss here the probability that an electron collision initiates ionic rotational excitation.

We assume that the initial vibrational state of the ion is $\{00^0\}$ and that the incident electron energy is less than 0.3 eV. The probability of the rotational excitation is given by the absolute square of the elements $\mathcal{S}_{N^+,K^+,v_1,v_2^{l_2};N^{+\prime},K^{+\prime},v_1',v_2'^{l_2'}}$, where both $\{v_1,v_2^{l_2}\}$ and $\{v_1',v_2'^{l_2'}\}$ vibrational states are $\{00^0\}$, and only the rotational states are different. The calculated probability of rotational excitation oscillates versus the electron energy due to the presence of many Rydberg states. The simplest quantity to use is the probability averaged over energy, which is almost energy independent in the region between the $\{00^0\}$ and $\{01^1\}$ vibrational levels. Here we present an alternative, simplified method to estimate this average probability analytically, which has been tested and found to give results very close to a full calculation.

Our simplified approach relies on an assumption that at the electron energies considered, the influence of excited vibrational levels on the averaged probability of rotational excitation is small. This assumption is validated by direct consideration of the corresponding matrix elements in Eq. (42) or else it can be derived by inspecting the photoionization spectra of H_3 [47,61]. Neglecting the influence of excited vibrational levels, the frame transformation of Eq. (42) can be evaluated analytically. At the first step, we evaluate the vibrational integral in Eq. (42). The result of this integration can be viewed as an effective scattering matrix $\overline{S}_{\Lambda,\Lambda}$, which is not very different from the $S_{\Lambda,\Lambda}(\mathcal{Q})$ matrix evaluated at the minimum of the ${H_3}^+$ potential. We can write

$$\mathcal{S}^{(N,K,m,l,G)}_{N^+,K^+;N^{+\prime},K^{+\prime}}=\sum_{\Lambda} C^{N^{+\prime},K^{+\prime}}_{l,-\Lambda;N,K}\overline{S}_{\Lambda,\Lambda}C^{N^+,K^+}_{l,-\Lambda;N,K}$$

$$=\sum_{\Lambda} C^{N^{+\prime},K^{+\prime}}_{l,-\Lambda;N,K}e^{2\pi i\overline{\mu}_\Lambda}C^{N^+,K^+}_{l,-\Lambda;N,K}, \qquad (43)$$

where $\overline{\mu}_\Lambda$ are quantum defects corresponding to the matrix $\overline{S}$. The nondiagonal elements of the scattering matrix $S_{\Lambda,\Lambda'}$ averaged over the $\{00^0\}$ vibrational states are identically zero. In the calculation we have used $\overline{\mu}_0=0.05$ and $\overline{\mu}_{\pm 1}=0.39$. The calculated rotationally inelastic collision probabilities for different symmetries and nuclear-spins of the ion are given in Table VI.

Now let us consider the results from H_3 photoionization experiments of Ref. [61]. The spectrum presented in that work (see Fig. 5 of Ref. [61]) showed the rotational autoionization of Rydberg states just below the excited, $N^+=3$, rotational state of the ortho ${H_3}^+$ ion. The lifetimes of these states are controlled by the same scattering matrix element $\mathcal{S}^{(N,K,m,l,G)}_{N^+,K^+;N^{+\prime},K^{+\prime}}$ that controls rotational excitation, although this is a scattering matrix in a closed channel, in the sense of multichannel quantum-defect theory. The same scattering matrix relevant at energies just above the rotational excitation threshold also controls the rotational autoionization just below the excited rotational threshold. Moreover, the probability of excitation $|\mathcal{S}|^2$ can be estimated approximately as the ratio of the widths of the rotationally autoionizing states to the separations between successive Rydberg levels. One can see from Fig. 5 of Ref. [61] that this ratio of widths to separations is of the order of unity for the rotationally autoionizing states. There are a few narrow perturbing lines, but those are vibrationally autoionizing states that are ignored for this analysis. Reference [61] can be viewed as an experimental confirmation of our theoretical logic.

VII. THE CROSS SECTION AND THE RATE OF DISSOCIATIVE RECOMBINATION

The scattering matrix $\mathcal{S}$ of Eq. (42) describes the electron-ion scattering when the electron energy is high enough for all collision channels to be open. The scattering matrix $\mathcal{S}^{phys}(E)$ for energies, when some channels are closed, is obtained by the "closed-channel-elimination" procedure [31]:

$$\mathcal{S}^{phys}(E)=\mathcal{S}^{oo}-\mathcal{S}^{oc}[\mathcal{S}^{cc}-e^{-2i\beta(E)}]^{-1}\mathcal{S}^{co}. \tag{44}$$

(see Eq. (2.50) of Ref. [31]). The matrix $\mathcal{S}^{phys}(E)$ has $N_o \times N_o$ dimensions, N_o being the number of open channels.

In Eq. (44), the collision energy E divides all channels as either energetically open or closed, N_o and $N_c=N_{tot}-N_o$. The matrices $\mathcal{S}^{oo}$, $\mathcal{S}^{oc}$, $\mathcal{S}^{cc}$, and $\mathcal{S}^{co}$ are corresponding parts of the original matrix $\mathcal{S}$ [11], written as

$$\mathcal{S}=\begin{pmatrix} \mathcal{S}^{oo} & \mathcal{S}^{oc} \\ \mathcal{S}^{co} & \mathcal{S}^{cc} \end{pmatrix}, \tag{45}$$

$\beta(E)$ is a diagonal $N_c \times N_c$ matrix:

$$\beta_{ij}(E)=\frac{\pi}{\sqrt{2(E_i-E)}}\delta_{ij}, \tag{46}$$

where E_i refers to a particular ionization threshold $i=\{v_1,v_2^{l_2}\}(N^+,K^+)$. For outgoing-wave Siegert states, the energy E_i is complex. Evaluating the square root in the above equation, we take the branch with the positive real part. It is consistent with the case when E_i has no imaginary part, i.e., corresponds to a bound state.

To calculate the cross section, we also need the conjugated scattering matrix. Because of the unusual orthonormality properties of the Siegert states, the conjugated scattering matrix $\mathcal{S}^\dagger$ is not simply the Hermitian conjugate of the matrix $\mathcal{S}$. More precisely, in addition to $\mathcal{S}^{phys}(E)$, we need a matrix $\mathcal{S}^{\dagger phys}(E)$ which is calculated in a way similar to $\mathcal{S}^{phys}(E)$ but with the complex-conjugated scattering matrix in Eq. (32):

$$S^\dagger_{v_1,v_2,l_2,\Lambda;v_1',v_2',l_2',\Lambda'}=\langle\psi_{v_1,v_2,l_2}(R)|S^{T*}_{v_2,l_2,\Lambda;v_2',l_2',\Lambda'}(R)| \times\psi_{v_1',v_2',l_2'}(R)\rangle_S. \tag{47}$$

In the above equation, the superscript T∗ implies the usual Hermitian conjugation, with both a transposition and a complex conjugation. However, the wave functions are not conjugated. The channel elimination Eq. (44) should also account for the complex conjugation by changing the sign of $\beta(E)$

$$\mathcal{S}^{\dagger phys}(E)=\mathcal{S}^{\dagger oo}-\mathcal{S}^{\dagger oc}[\mathcal{S}^{\dagger cc}-e^{2i\beta(E)}]^{-1}\mathcal{S}^{\dagger co}. \tag{48}$$

(It is important *not* to complex conjugate β in this expression.)

Once the scattering matrices $\mathcal{S}^{phys}(E)$ and $\mathcal{S}^{\dagger phys}(E)$ are calculated, the raw dissociative recombination cross section is extracted from the "unitarity defect" of the relevant column of the scattering matrix:

$$\sigma(E_{el})=\frac{\pi}{2E}\left(1-\sum_{i=1,N_o}\mathcal{S}^{phys}_{i,i'}(E)\mathcal{S}^{\dagger phys}_{i',i}(E)\right),$$

$$E_{el}=E-E_{i'}. \tag{49}$$

In calculation, the term $\Sigma\mathcal{S}^{phys}_{i,i'}(E)\mathcal{S}^{\dagger phys}_{i',i}(E)$ is always real, positive, and it is found not to exceed unity, to a good numerical accuracy. In this energy range all open ionization channels i have a real energy $E_{i'}$.

In the above equation, i' is the electron entrance channel and E_{el} is the asymptotic electron energy. In the storage-ring experiments [1,3,62–66], the entrance channel is the ground vibrational ionic state, the rotational quantum number can be different: $i'=\{0,0^0\}(N^+,K^+)$. Since the scattering matrices $\mathcal{S}^{phys}(E)$ and $\mathcal{S}^{\dagger phys}(E)$ and the cross section of Eq. (49) are calculated for a good total molecular angular momentum N, the total symmetry $\Gamma=A_2'$ or $\Gamma=A_2''$, and the total nuclear-spin $I=1/2$ or $I=3/2$, we will assign these three labels to the symbol of the cross section $\sigma_{\Gamma,I,N}(E_{el})$. To obtain the experimentally measured cross section $\sigma_{\Gamma,I}(E_{el})$, we should average over different initial states (m^+) and sum up over the final states (N and m) of the system:

$$\sigma_{\Gamma,I}(E_{el})=\frac{1}{2N^++1}\sum_N(2N+1)\sigma_{\Gamma,I,N}(E_{el}). \tag{50}$$

The symmetry label Γ and the total nuclear-spin are still definitive quantum numbers for the cross section $\sigma_{\Gamma,I}(E_{el})$. In the above sum, N varies from 0 or N^+-1 to N^++1.

The corresponding rate $\alpha(E_{el})$ is obtained by multiplying the cross section by velocity:

$$\alpha(E_{el})=\sqrt{2E_{el}}\sigma(E_{el}). \tag{51}$$

When rotationally excited states of $H_3{}^+$ are present, the rate should be averaged over the initial distribution of the rotational states. Assuming the thermally averaged rotational excitation of the gas with the temperature T_{rot}, the rotationally averaged rate is

$$\alpha_{\Gamma,I,T_{rot}}(E_{el})=\frac{\sum_{N^+}(2N^++1)\exp\left[-\frac{E(N^+)}{kT_{rot}}\right]\alpha_{\Gamma,I}(E_{el})}{\sum_{N^+}(2N^++1)\exp\left[-\frac{E(N^+)}{kT_{rot}}\right]}, \tag{52}$$

where $E(N^+)$ is the energy of the rotational level (N^+,K^+). Typically, excited rotational levels should be taken into account if the rotational temperature is higher than 150 K.

There are four distinguishable species allowed for ${H_3}^+$: the total molecular symmetry Γ can be A_2' or A_2'' and the total spin can be $I=1/2$ or 3/2. The change of the species is generally possible only via chemical reactions when one proton is cut off and then is attached again to the two other protons. This interconversion process is believed not to occur in the diffuse interstellar clouds and in the storage-ring experiment, but it certainly can occur in dense interstellar clouds where H_2 molecule is abundant [57,58,67]. This interconversion can also occur in storage-ring experiments. Besides chemical reactions, the A_2' and A_2'' states of the same nuclear-spin are connected by the so-called "forbidden" rotational transitions. In the present calculations, we included two rotational states for every species. Therefore, for the ground vibrational level, we included the following states with energies:
(1,1)[$I=1/2$]0 cm^{-1}; (2,1)[$I=1/2$] 173.23 cm^{-1};
(1,0)[$I=3/2$] 22.84 cm^{-1}; (3,0)[$I=3/2$] 452.75 cm^{-1};
(2,2)[$I=1/2$] 105.17 cm^{-1}; (3,2)[$I=1/2$] 363.89 cm^{-1};
(3,3)[$I=3/2$] 251.22 cm^{-1}; (4,3)[$I=3/2$] 594.57 cm^{-1}
[57–60]. This set of rotational levels allows us to account properly for the rotational temperatures of the ion up to 600 K.

For astrophysical purposes, one determines the rate coefficient $\alpha(kT)$ averaged over the Maxwellian distribution of electrons at the temperature T [1,68]:

$$\alpha_{th}(kT)=\frac{8\pi}{(2\pi kT)^{3/2}}\int_0^\infty \alpha(E_{el})e^{-E/kT}\sqrt{\frac{1}{2}E_{el}}dE_{el}. \tag{53}$$

In the interstellar medium, the rotational ionic temperature is the same as the electron temperature. If we assume that species having different total nuclear-spin are in thermal equilibrium as well—i.e., since chemical interconversion is possible—the corresponding generalization of formula (53) is given by

$$\alpha_{th}(kT)=\frac{1}{\mathcal{N}_\Sigma}\frac{8\pi}{(2\pi kT)^{3/2}}\int_0^\infty\sum_{N^+,s}\alpha_{\Gamma,I,N^+}(E)w(N^+,s,T)\times e^{-E_{el}/kT}\sqrt{\frac{1}{2}E_{el}}dE_{el}, \tag{54}$$

where the thermal weights $w(N^+,s,T)$ account for the relative contribution of a particular rotational level at a given temperature T. The index s numerates the four mentioned species $A_2'[3/2]$, $A_2''[3/2]$, $A_2'[1/2]$, and $A_2''[1/2]$, allowed for the ground vibrational level. The weights and corresponding normalization factor $\mathcal{N}_\Sigma$ are

$$w(N^+,s,T)=(2I+1)(2N^++1)e^{-E_R(I,\Gamma,N^+)/kT},$$

$$\mathcal{N}_\Sigma=\sum_{N^+,s}w(N^+,s,T). \tag{55}$$

Rotational energies $E_R(I,\Gamma,N^+)$ of eight levels included in the thermal averaging are given above.

Equation (54) gives the dissociative recombination rate as a function of temperature when electron energy is in thermal equilibrium with rotational and nuclear-spin distributions of ${H_3}^+$ ions. In the storage-ring experiments [1,62,63], certain degrees of freedom are not in thermal equilibrium. The electron energy is not distributed uniformly with directions in space. One space component, namely, the parallel energy $E_\parallel$, is very well controlled. The distribution along this component is essentially a δ function. However, there is a non-negligible energy spread $\overline{E_\perp}$ for the electron motion in the two other perpendicular directions. This energy spread has to be accounted for when experimental and theoretical results are compared. Following Ref. [1], we assume a Maxwellian energy distribution along these two directions. There is one more characteristic energy distribution in the storage-ring experiment, namely, the rotational temperature T_{rot} of the ions. In general, T_{rot} is independent of $\overline{E_\perp}$ and has to be accounted for separately. These considerations are accounted for by the following averaging procedure:

$$\alpha_{sr}(E_\parallel)=\frac{1}{\mathcal{N}_1}\int_0^\infty dE_\perp w_1(E_\perp)\frac{1}{\mathcal{N}_2}\sum_{I,\Gamma,N^+}w_2(I,\Gamma,N^+,T)\times\alpha_{\{\Gamma,I,N^+\}}(E_\perp+E_\parallel), \tag{56}$$

where the weights $w_1(E_\perp)$ and $w_2(\Gamma,I,N^+,T)$ are determined by the corresponding mean values $\overline{E_\perp}$ and kT_{rot} for electron energy and rotational energy distributions,

$$w_1(E_\perp)=\exp\left(-\frac{E_\perp}{\overline{E_\perp}}\right),$$

$$w_2(\Gamma,I,N^+,T)=(2I+1)(2N^++1)\exp\left(-\frac{E_R(I,\Gamma,N^+)}{kT_{rot}}\right). \tag{57}$$

The two normalization factors $\mathcal{N}_1$ and $\mathcal{N}_2$ are determined by

$$\mathcal{N}_1=\int_0^\infty dE_\perp w_1(E_\perp)=\overline{E_\perp},$$

$$\mathcal{N}_2=\sum_{I,\Gamma,N^+}w(I,\Gamma,N^+,T). \tag{58}$$

The total total energy E in Eq. (56), at which the rate $\alpha_{\{\Gamma,I,N^+\}}$ enters into the formula, is now expressed as $E=E_\perp+E_\parallel$.

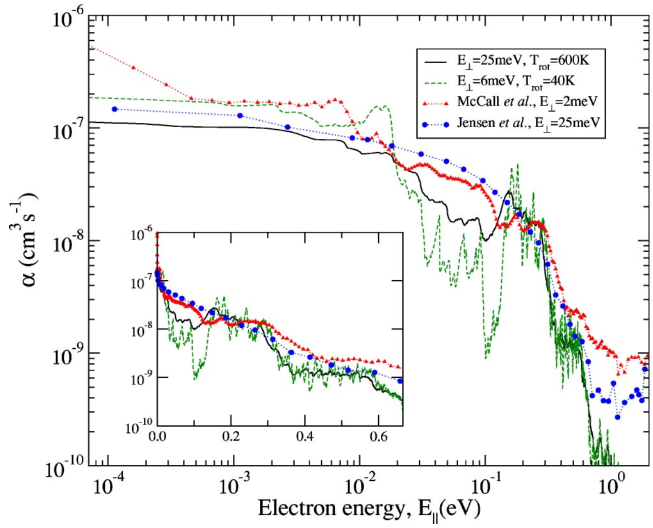

FIG. 8. Comparison of theoretical and experimental rates of dissociative recombination. The theoretical rate (solid and dashed lines) is shown as a function of the parallel electron energy $E_\parallel$. In the theoretical curves (present work), the rate has been averaged over the lowest states, for two different values of the transverse energy spread, $\overline{E_\perp}=6$ meV (dashed curve) and 25 meV (solid curve). Also shown are the data from two different storage-ring experiments. The experimental data from Ref. [66] ($\overline{E_\perp}=2$ meV) is shown as triangles, and, another recent measurement from Ref. [62] ($\overline{E_\perp}=25$ meV) is shown as circles. Both theoretical curves are averaged over a Boltzmann distribution for the rotational levels of the ion, including both the ortho and para symmetries. The calculated curves reproduce most of the major features of the experimental rate.

VIII. DISCUSSION OF CALCULATED RESULTS

Figure 8 shows our calculated rates for two different conditions (dashed and solid lines) as functions of the relative electron energy $E_\parallel$, compared with data from two storage-ring experiments, circles [62] and triangles [66]. The calculated rate coefficient is averaged over the experimental energy spread $\overline{E_\perp}$ and over the rotational energy kT_{rot} of the H_3^+ ions, using the formulas discussed above. However, in the calculation, which should be compared with the experimental results by McCall *et al.*, we use a larger energy spread $\overline{E_\perp}=6$ meV than the experimental value $\overline{E_\perp}=2$ meV. The quoted experimental resolution $\overline{E_\perp}=2$ meV would give many more resonances, which are not observed experimentally. Thus, the solid curve is calculated using $\overline{E_\perp}=6$ meV and should be compared with the experimental data [66] represented with triangles. We have also compared our theoretical results with another storage-ring experiment by Jensen *et al.* [62] (circles in Fig. 8). In this experiment, $\overline{E_\perp}=25$ meV. Thus, we have calculated a second theoretical curve with the quoted value of $\overline{E_\perp}$. The experimental resolution in $E_\parallel$ is estimated in Ref. [66] to be $\Delta E_\parallel \approx 0.1$ meV. This is sufficiently smaller than $\Delta E_\perp$ that we have not carried out in the corresponding convolution over $E_\parallel$. The result is represented by a dashed curve in Fig. 8.

In some region between 0.04 eV and 0.1 eV, the theoretical rate is significantly lower than the measured rate, although the theoretical curves exhibit similarities to the general behavior of the experimental rate in these regions. We cannot point out the cause of this disagreement with any certainty, but one possibility is that some higher rotational levels may still be present in the storage-ring experiments, either when the beam emerges from the source or else perhaps through an excitation process after the ions are in the ring and have passed through the electron interaction region one or more times. Our calculations for excited rotational states of the ion show that this gap tends to be filled up if the next rotational states are included in our calculation. The rotational temperature of H_3^+ in the storage-ring experiment by Jensen *et al.* [62] may be as high as 2700 K [69]. Our calculation at $T_{rot}=600$ K (the highest T_{rot} we can treat using only eight rotational levels of the ground vibrational state) shows a better agreement with the experiment of Ref. [62], shown in Fig. 8. In the experiment of Ref. [66], the initial rotational temperature of ions is measured to be much lower (20–60 K). The data from this experiment display the dip around 0.1 eV, but it is not as wide and pronounced as in the theoretical curve.

The theoretical curves also differ from the experimental results in their much greater number and depth of resonances. The experimental curve with high rotational temperature shows virtually no resonances. The corresponding theoretical curve calculated for the higher rotational temperature exhibits some resonances, although they are largely washed out. The new experimental curve at a low rotational temperature shows some resonances, but far fewer than what we predict should be observable at the experimental resolution. This systematic discrepancy between theoretical and experimental results, i.e., in the number and prominence of these resonances, is simply not yet understood. However, analogous discrepancies are familiar in many other comparisons between the DR theory and the experiment, including even simple diatomic targets such as H_2^+ [8,12].

There remains some uncertainty about the distribution of population among various rovibrational levels of H_3^+, because rotational excitations could occur when the ions pass through the electron beam. Figure 9 provides a breakdown of the DR rates for the lowest four levels relevant. Interestingly, the curve that resembles the newest DR experiment [66] is the one in which H_3^+ is initially in the para (22) state. The agreement with the experiment is noticeably better, around $E_\parallel=0.1$–2.5 meV, 10–100 meV, and 0.2–0.4 eV as well. The better agreement with the (22) theoretical DR rate may be fortuitous. On the other hand, it may point to the desire of measuring the rovibrational H_3^+ distribution while the ions are actually inside the storage-ring.

Figure 10 demonstrates the thermally averaged DR rate (solid black curve) for the thermal distribution of collision energies as a function of temperature. This curve is the most relevant in astrophysical observations of H_3^+, because the rotational temperature T_{rot} of the ions is chosen equal to the electron temperature T_{el}. The theoretical (solid) curve displays a plateaulike behavior, which differs from the experimental (dot-dashed) curve [66] at low temperatures. This dif-

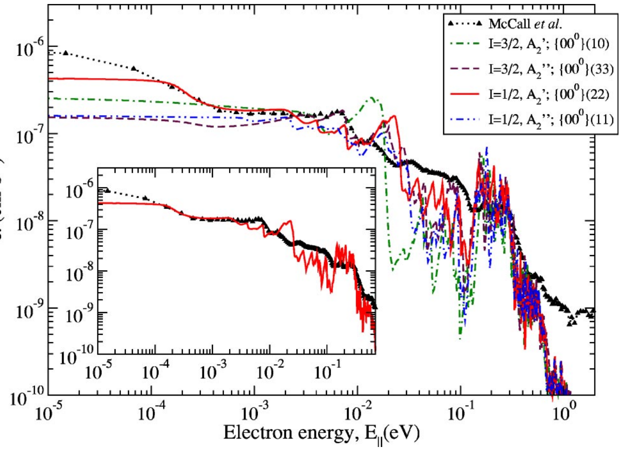

FIG. 9. This figure gives DR rates calculated separately for each symmetry specified by quantum numbers I and Γ (rotational and vibrational quantum numbers are also specified). These rates would correspond to a situation in which the $H_3{}^+$ ion is prepared in the single rovibrational state specified. The theoretical curves are convolved with $\overline{E_\perp}=6$ meV. For comparison, we also plot the experimental curve (triangles) from Ref. [66]. The inset shows the experimental DR rate and the rate for the initial state $\{00^0\}(22)$ state alone. This rate displays a better agreement with experiment than the DR rate averaged over all four symmetries (see Fig. 8).

ference is caused partly by the fact that the limiting low-energy behavior of the DR rate is not achieved until surprisingly low incident energies, well below the measured range. The double-dot-dashed curve is our calculation using parameters that correspond to the conditions of the newest experiment [66], where only the two lowest states are populated with constant relative contributions corresponding to the constant rotational temperature $T_{rot}=20$–60 K. The theoretical (double-dot-dashed) curve is calculated at $T_{rot}=40$ K. The two dashed curves represent the rate averaged thermally over the ionic rotational and the electron energy distributions, calculated separately for the ortho and para spin states.

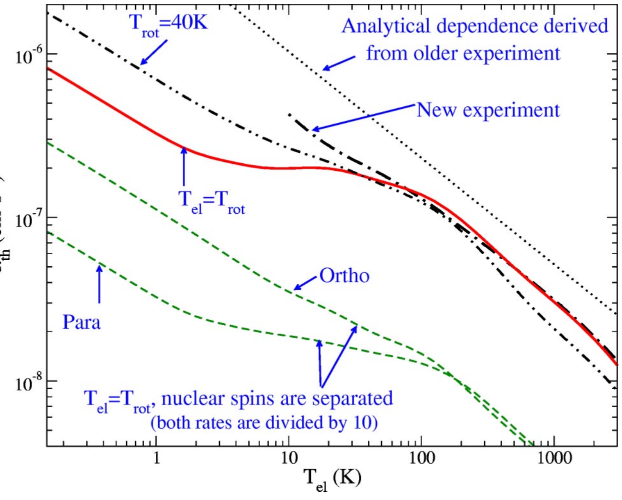

FIG. 10. The theoretical thermally averaged recombination rate (solid line) is shown as a function of temperature. This curve is the one most relevant to compare with astrophysical observations of $H_3{}^+$, because the rotational temperature T_{rot} of the ions is equal to the electron temperature T_{el}. At 300 K the theoretical thermal rate is $\alpha_{th}=7.2\pm1.1\times10^{-8}$ cm^3/s. The thick dashed-dotted curve represents the experimentally extracted thermal rate [66], which can be compared with our double-dotted-dashed curve calculated for their stated ion source conditions.

The reason why stationary afterglow experiments [70] measure such a low DR rate remains a problem. In view of the presence of perturbing species in the vicinity of the recombining ions and the vital role of easily affected Rydberg state pathways, it seems plausible that these controlling contributions might be modified in an afterglow experiment. A detailed model of pressure or field effects on these pathways remains a desirable goal for future investigations. On the other hand, a flowing afterglow experiment [71] gives a rate coefficient $\alpha_{th}(300\text{ K})=7.8\pm2.3\times10^{-8}$ cm^3/s which is in good general agreement with our rate $\alpha_{th}=7.2\times10^{-8}$ cm^3/s calculated at 300 K. One may also compare with the experimental results of Ref. [72], although the final measured rate was left somewhat ambiguous in that study.

IX. CALCULATION FOR $D_3{}^+$

A. Differences between our treatment of DR in $D_3{}^+$ and $H_3{}^+$

Using the method developed to calculate the DR rate for $H_3{}^+$, we have also calculated the rate for the $D_3{}^+$ ion. In this calculation, we use the same ionic potential surface and the same Jahn-Teller parameters as in the case of $H_3{}^+$. This is a good approximation, since the ionic potential surface and the Jahn-Teller parameters were calculated assuming infinite nuclear mass. Differences between these two ions first arise in our method when the adiabatic hyperspherical potential curves are calculated, since they depend on the mass of the nuclei and are therefore different for $D_3{}^+$.

Moreover, the deuterium nucleus is a boson in contrast to the fermionic nucleus of hydrogen. Therefore, the total nuclear-molecular symmetry of $D_3{}^+$ can only be A_1' or A_1'': any permutation of these identical nuclei should leave the total wave function unchanged. Again, as in the case of $H_3{}^+$, we construct symmetry-adapted combinations of nuclear-spin functions. Since the spin i of the deuteron is 1, there are more possible symmetries of the total nuclear-spin $\vec{I}=\vec{i}_1+\vec{i}_2+\vec{i}_3$ than in the case of $H_3{}^+$.

Each nucleus can be in one ($|\alpha\rangle$) of the three states depending on the projection of its spin on a fixed axis. We will refer the three states as $|-1\rangle$, $|0\rangle$, and $|1\rangle$. A symmetry-adapted nuclear-spin function of $D_3{}^+$ is constructed from products of the type $|\alpha\beta\gamma\rangle=|\alpha\rangle|\beta\rangle|\gamma\rangle$, where the first factor $|\alpha\rangle$ relates to the nucleus 1, the second factor to the nucleus 2, and the third term relates to the nucleus 3. For example, operation (12) applied to function $|\alpha\beta\gamma\rangle$ gives $|\beta\alpha\gamma\rangle$. The total number of nuclear-spin states is $3^3=27$.

We consider the case where all projections are the same, i.e., all three nuclei are in the same state. The total state can be written as $|\alpha\alpha\alpha\rangle$, which is totally symmetric under all permutations, and therefore belongs to the A_1 symmetry. There are three such products.

When two nuclei have the same spin projections and the third nucleus has a different projection, the total state being of the type $|\alpha\alpha\beta\rangle$, we construct linear combinations in the similar way as done for $H_3{}^+$ [see Eqs. (8) and (9)]. Thus, these products with fixed values of α and β transform according to either the A_1 or the E representation. There are six different combinations of α and β. Thus, the whole set of functions of the type $|\alpha\alpha\beta\rangle$ is decomposed into irreducible representations according to $6A_1\oplus 6E$.

We have only one possible set of spin projections that produce functions of the type $|\alpha\beta\gamma\rangle$ where all three factors are different. Permutations of the factors give six different products. Symmetry-adapted combinations of the functions can be made using the projector operators. We give only the final linear combinations

$$\begin{aligned}
A_1&:\frac{1}{\sqrt{6}}(|\alpha\beta\gamma\rangle+|\beta\alpha\gamma\rangle+|\beta\gamma\alpha\rangle+|\gamma\beta\alpha\rangle+|\gamma\alpha\beta\rangle\\
&\quad+|\alpha\gamma\beta\rangle),\\
A_2&:\frac{1}{\sqrt{6}}(|\alpha\beta\gamma\rangle-|\beta\alpha\gamma\rangle+|\beta\gamma\alpha\rangle-|\gamma\beta\alpha\rangle+|\gamma\alpha\beta\rangle\\
&\quad-|\alpha\gamma\beta\rangle),\\
E_A(1)&:\frac{1}{\sqrt{12}}(2|\alpha\beta\gamma\rangle+2|\beta\alpha\gamma\rangle-|\beta\gamma\alpha\rangle-|\gamma\beta\alpha\rangle-|\gamma\alpha\beta\rangle\\
&\quad-|\alpha\gamma\beta\rangle),\\
E_B(1)&:\frac{1}{\sqrt{4}}(|\beta\gamma\alpha\rangle-|\gamma\beta\alpha\rangle+|\gamma\alpha\beta\rangle-|\alpha\gamma\beta\rangle),\\
E_A(2)&:\frac{1}{\sqrt{4}}(|\beta\gamma\alpha\rangle+|\gamma\beta\alpha\rangle-|\gamma\alpha\beta\rangle-|\alpha\gamma\beta\rangle),\\
E_B(2)&:\frac{1}{\sqrt{12}}(2|\alpha\beta\gamma\rangle-2|\beta\alpha\gamma\rangle-|\beta\gamma\alpha\rangle+|\gamma\beta\alpha\rangle-|\gamma\alpha\beta\rangle\\
&\quad+|\alpha\gamma\beta\rangle).
\end{aligned}\tag{59}$$

Thus, the functions of the type $|\alpha\beta\gamma\rangle$ form the representation $A_1\oplus A_2\oplus 2E$.

The final result is that the group of permutation of three particles with spin 1 generates the representation $10A_1\oplus A_2\oplus 8E$. Let us now consider the statistical weights of these states. Since the E representation is two dimensional, $10A_1\oplus A_2\oplus 8E$ gives 27 states in agreement with the total number of nuclear states. Calculating the scattering matrix for the total nuclear-molecular wave function having E nuclear symmetry (in this case, the rovibrational symmetry is also E) of $D_3{}^+$, we treat both E components simultaneously. Thus, in the final averaging over nuclear-spin states, the nuclear statistical weights are given just by multiplicity factors in the representation $10A_1\oplus A_2\oplus 8E$, i.e., $10:1:8$.

Since the total nuclear-molecular function can be of A_1' or A_1'' symmetry, and the nuclear wave function can be of A_1, A_2, or E symmetry, all six D_{3h} representations of rovibrational functions are allowed in the case of $D_3{}^+$. It means that all possible combinations of vibrational and rotational wave functions are allowed: there is always a nuclear-spin state which can produce the right total symmetry. For example, for $D_3{}^+$, the state $\{00^0\}(00)$ is allowed. There is one more difference in construction of the total rovibrational-nuclear functions of $D_3{}^+$ compared to $H_3{}^+$. Equation (13) should be modified to impose the overall total A_1' or A_1'' symmetry. Instead of the minus sign in Eq. (13), there should be a plus sign.

For calculating the $H_3{}^+$ DR rate, we used the rovibrational energies determined in experiments and the accurate *ab initio* calculation [57,59,60]. In the present calculation of the $D_3{}^+$ DR rate, we use approximative rovibrational energies. Vibrational energies of levels $\{v_1v_2^{l_2}\}$ are determined from the two-step procedure to diagonalize the vibrational Hamiltonian of $D_3{}^+$. This procedure was described in Sec. IV C. Then the rovibrational energies of $\{v_1v_2^{l_2}\}(N^+,K^+)$ are determined by adding a rotational correction $E[\{v_1v_2^{l_2}\}(N^+,K^+)]$. We have used a very rough approximation for this term, namely, $E[\{v_1v_2^{l_2}\}(N^+,K^+)]=B_vN^+(N^++1)$. We could use a more elaborate approximation, for example, as in Ref. [44], but the corresponding correction is much smaller than the error in vibrational energies due to the two-step adiabatic treatment. In our calculation we use the rotational constant $B_v=20\ \text{cm}^{-1}$ independent of the vibrational and rotational quantum numbers.

B. Results for $D_3{}^+$

Results of the calculation for $D_3{}^+$ are shown in Fig. 11 as solid and dashed lines. The solid line shows the rate calculated for the experimental conditions of Larsson *et al.* [73] (triangles in the figure). In the experiment, the perpendicular energy resolution $E_\perp$ is 10 meV; the rotational temperature is high, around 1000 K or more. The theoretical curve is calculated for $E_\perp=10$ meV and $T_{rot}=600$ K. The figure also shows the comparison of the theoretical results (dashed line) with another experiment [64] (circles). In Ref. [64], the experimental energy dependence of the rate is given in relative units. To obtain the absolute value of the experimental dependence, we calibrated the rate from Ref. [64] to the absolute experimental DR rate for $D_3{}^+$ measured by Larsson *et al.* [73]. The calibration was made for a value of the rate at quite high energy, 10 eV, where both experiments give presumably the same reliable results. Therefore, the circles in Fig. 11 represent the calibrated curve. No rotational and electron resolutions are specified for this experiment as well. We assume that the rotational temperature is comparably as high as in the experiment by Larsson *et al.* [73]. The electronic resolution $E_\perp$ can be roughly estimated from the behavior of the curve at low $E_\parallel$ energies. We estimated this resolution to be around 40 meV. Thus, the corresponding theoretical curve is calculated with the parameters $E_\perp=40$ and $T_{rot}=600$ K.

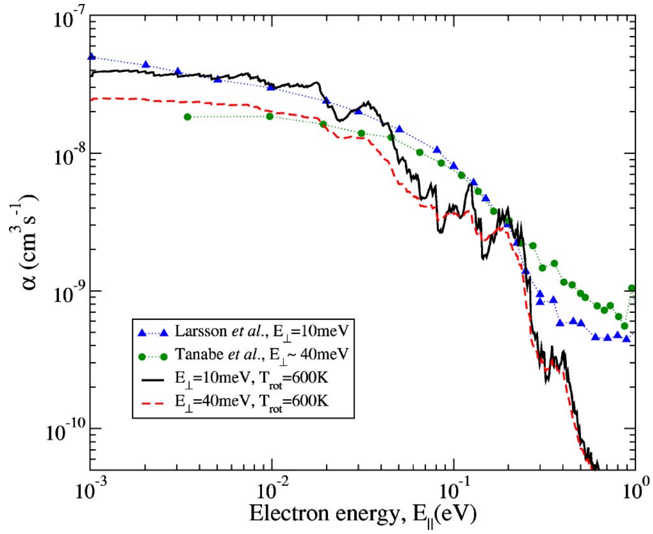

FIG. 11. Comparison of calculated (solid and dashed lines) and experimental (circles and triangles) rates of dissociative recombination for D_3^+. All rates are shown as functions of the parallel electron energy $E_\parallel$. The experimental data from the experiment by Larsson *et al.* [73] (triangles) should be compared with the theoretical rate (solid line) calculated for the stated experimental conditions. The second experimental data by Tanabe *et al.* [64] (circles) should be compared with theoretical rate represented by the dashed line.

Summarizing the results for D_3^+, we conclude that the agreement between theory and experiment for the D_3^+ ion is comparable or better to that found for H_3^+. A good general agreement is found between the storage-ring experiment and the theory. The main discrepancy in the theoretical curves is the presence of two deep minima around 0.09 and and 0.17 eV, which are absent in the experimental results from the storage-rings [64,73]. On the other hand, the merged electron-ion-beam experiment [77] does show at least one deep minimum around the right energy, although it could be fortuitous because at higher energies >0.2 eV this experiment manifests an unreasonably high rate. Note that in contrast to H_3^+, the D_3^+ theoretical rate curves do not display very deep minima. This is simply due to the fact that we used a larger value of $E_\perp$ for the D_3^+ theoretical curves than for the H_3^+ ion. Finally, as was found for the H_3^+ ion, the calculated and experimental curves differ significantly at energies above 0.4 eV.

X. SUMMARY AND CONCLUSIONS

In conclusion, we summarize a number of key issues that have emerged from the present study. These are given as follows.

(1) For many years theory failed to explain the relatively high rate of dissociative recombination of H_3^+ with electrons. Theory predicted the rate to be lower by several orders of magnitude that the experiments regarded generally as the most reliable. We have shown that the Jahn-Teller coupling, previously neglected in theoretical studies, plays a crucial role in the process and generates a relatively high rate. Our theoretical DR rate is in good agreement with the storage-ring experiments [62,63,66]. There are still regions of disagreement, although they are far smaller than in previous theoretical studies. The main disagreement with the experiment is the presence of pronounced resonances in the theoretical rate. The experimental rate exhibits some resonances too, but they are less numerous and shallower than the theoretical resonances. Hopefully, future studies will clarify the origin of this discrepancy. The thermally averaged rate does not manifest any resonances, in either the theory or the experiment. The agreement between theory and the storage-ring experiments for the thermally averaged rate is good at temperatures larger than 30 K. Below this temperature, theoretical and experimental results diverge. One possible reason for the low-temperature disagreement might be the fact that the experimental rate for low temperatures should be considered as extrapolated. Our treatment has allowed us to calculate the rate of D_3^+ dissociative recombination as well. For D_3^+, we have obtained even better agreement with storage-ring experiments [64,73]. Although theory predicts the presence of resonances for D_3^+ too, these resonances are not as deep as for H_3^+. The experiments with D_3^+ exhibit no resonance at all below 2 eV incident electron energy, perhaps because these experiments have been performed with presumably hot rotational ions.

(2) Besides neglecting the Jahn-Teller effect, the previous theoretical studies did not consider the full treatment of three-dimensional vibrational dynamics of H_3^+. In the present treatment, we have considered the complete three-dimensional vibrational dynamics. It turns out that inclusion of all three vibrational degrees of freedom is essential to account properly for the nonadiabatic electron-nuclear coupling. In H_3, this coupling is described in terms of Jahn-Teller parameters: electronic and nuclear motions are strongly coupled through the E vibrational and electronic states. The E vibrational states involve motion at least in the two-dimensional space: the space of two hyperangles in our case. A third coordinate, namely, the hyperradius, is necessary to represent dissociation. Therefore, we surmise that any reduced-dimension approach will struggle to describe the H_3^+ DR process.

(3) To the best of our knowledge, this is the first method able to treat DR in triatomic molecules including all the degrees of freedom of the electron-ion complex. The method treats the electron-ion interaction, including all vibrational and rotational motions of the ion. It accounts for all symmetry restrictions, including rotational, vibrational, and nuclear-spin symmetries. We should point out that the inclusion of nuclear-spin symmetries gives improved agreement with experiment, but it is not as crucial as the inclusion of Jahn-Teller physics. The results shown in Fig. 8 for individual symmetries suggest that it is proper to test the actual rovibrational H_3^+ distribution inside the storage ring, while the electron beam is on.

(4) The method described in this work was developed for H_3^+ DR, but it can be used for some other similar systems. For other molecules of D_{3h} symmetry, such as the NH_3^+ molecule, the method can be applied with appropriate

changes. The main modifications should be in the ionic vibrational potential and in the quantum-defect parameters. The method can be modified to treat DR in linear molecules as well. We also stress that processes besides dissociative recombination can be treated. We have applied it to interpret photoabsorption and photoionization experiments with the H_3 molecule [47,61], but those results will be discussed in a subsequent paper.

Although this study presents the progress in the controversial problem of DR in ${H_3}^+$, there are still some interesting issues. At present, the main problem is a disagreement between the ${H_3}^+$ DR rates in storage-ring experiments and in recent experiments by Glosík *et al.* [70,74–76] a stationary afterglow plasma. The results of Glosík and co-workers suggest that the rate is at least 20 times smaller than in the storage-ring experiments. They have also found a strong dependence of the DR rate on the concentration of H_2 molecules. At high H_2 densities, the afterglow plasma experiments give DR rate in good agreement with the storage-ring experiments and with the present calculations for ${H_3}^+$ and ${D_3}^+$. At low H_2 densities, the DR rate in the afterglow plasma experiments is diminishing to very low values. This dependence has not yet been explained in the framework of the present theoretical approach.

ACKNOWLEDGMENTS

This work has been supported in part by the NSF, by the U.S. Department of Energy (Office of Science), and by an allocation of NERSC supercomputing resources. The authors are grateful to G. Dunn, J. Hutson, M. Larsson, and J. Stephens for fruitful discussions and to E. Hamilton and B. Esry for assistance and access to their unpublished results.

---

[1] G. Sundström, J.R. Mowat, H. Danared, S. Datz, L. Broström, A. Filevich, A. Källberg, S. Mannervik, K.G. Rensfelt, P. Sigray, M. af Ugllas, and M. Larsson, Science **263**, 785 (1994).
[2] T. Oka, Philos. Trans. R. Soc. London, Ser. A **358**, 2363 (2000).
[3] M. Larsson, Philos. Trans. R. Soc. London, Ser. A **358**, 2433 (2000).
[4] A.E. Orel, I.F. Schneider, and A. Suzor-Weiner, Philos. Trans. R. Soc. London, Ser. A **358**, 2445 (2000).
[5] B.J. McCall and T. Oka, Science **287**, 1941 (2000).
[6] A. Suzor-Weiner and I.F. Schneider, Nature (London) **412**, 871 (2001).
[7] A. Giusti, J. Phys. B **13**, 3867 (1980).
[8] A. Giusti-Suzor, J.N. Bardsley, and C. Derkits, Phys. Rev. A **28**, 682 (1983).
[9] A. Giusti-Suzor and Ch. Jungen, J. Chem. Phys. **80**, 986 (1984).
[10] Ch. Jungen, Phys. Rev. Lett. **53**, 2394 (1984).
[11] C.H. Greene and Ch. Jungen, Adv. At. Mol. Phys. **21**, 51 (1985).
[12] A.P. Hickman, J. Phys. B **20**, 2091 (1987).
[13] Ch. Jungen, *Molecular Applications of Quantum Defect Theory* (Institute of Physics, Bristol, 1996).
[14] Ch. Jungen and S.C. Ross, Phys. Rev. A **55**, R2503 (1997).
[15] A. Matzkin, Ch. Jungen, and S.C. Ross, Phys. Rev. A **62**, 062511 (2000).
[16] V. Kokoouline and C.H. Greene, Phys. Rev. Lett. **90**, 133201 (2003).
[17] J.A. Stephens and C.H. Greene, Phys. Rev. Lett. **72**, 1624 (1994).
[18] J.A. Stephens and C.H. Greene, J. Chem. Phys. **102**, 1579 (1995).
[19] I.F. Schneider, A.E. Orel, and A. Suzor-Weiner, Phys. Rev. Lett. **85**, 3785 (2000).
[20] M. Tashiro and S. Kato, Chem. Phys. Lett. **354**, 14 (2002).
[21] M. Tashiro and S. Kato, J. Chem. Phys. **117**, 2053 (2002).
[22] R.T. Pack and G.A. Parker, J. Chem. Phys. **87**, 3888 (1987).
[23] B.D. Esry, C.D. Lin, and C.H. Greene, Phys. Rev. A **54**, 394 (1996).
[24] B.K. Kendrick, R.T. Pack, R.B. Walker, and E.F. Hayes, J. Chem. Phys. **110**, 6673 (1999).
[25] D. Blume and C.H. Greene, J. Chem. Phys. **112**, 8053 (2000).
[26] D. Blume, C.H. Greene, and B.D. Esry, J. Chem. Phys. **113**, 2145 (2000).
[27] B.D. Esry, C.H. Greene, and H. Suno, Phys. Rev. A **65**, 010705 (2001).
[28] V. Kokoouline, C.H. Greene, and B.D. Esry, Nature (London) **412**, 891 (2001).
[29] E.L. Hamilton and C.H. Greene, Phys. Rev. Lett. **89**, 263003 (2002).
[30] T.F. O'Malley, Phys. Rev. **150**, 14 (1966).
[31] M. Aymar, C.H. Greene, and E. Luc-Koenig, Rev. Mod. Phys. **68**, 1015 (1996).
[32] J.H. Macek, J. Phys. B **1**, 831 (1968).
[33] Y. Zhou, C.D. Lin, and J. Shertzer, J. Phys. B **26**, 3937 (1993).
[34] C.D. Lin, Phys. Rep. **257**, 1 (1995).
[35] P. Siegbahn and B. Liu, J. Chem. Phys. **68**, 2457 (1978).
[36] D.G. Truhlar and C.J. Horowitz, J. Chem. Phys. **68**, 2466 (1978).
[37] A.J.C. Varandas, F.B. Brown, C.A. Mead, D.G. Truhlar, and N.C. Blais, J. Chem. Phys. **86**, 6258 (1987).
[38] A. Staib, W. Domcke, and A.L. Sobolewski, Z. Phys. D: At., Mol. Clusters **16**, 49 (1990).
[39] A. Staib and W. Domcke, Z. Phys. D: At., Mol. Clusters **16**, 275 (1990).
[40] U. Fano, Phys. Rev. A **2**, 353 (1970).
[41] P. Bunker and P. Jensen, *Molecular Symmetry and Spectroscopy* (NRC Research Press, Ottawa, 1998).
[42] R. Reichle, Ph.D. thesis, University of Freiburg, Freiburg, 2002 (unpublished).
[43] D.A. Varshalovich, A.N. Moskalev, and V.K. Khersonskii, *Quantum Theory of Angular Momentum* (World Scientific, Singapore, 1988).
[44] J.K.G. Watson, Philos. Trans. R. Soc. London, Ser. A **358**, 2371 (2000).
[45] J.K.G. Watson, J. Mol. Spectrosc. **103**, 350 (1984).

[46] H.C. Longuet-Higgins, in *Advances in Spectroscopy*, edited by H.W. Thompson (Interscience, New York, 1961), Vol. II, p. 429.

[47] I. Mistrík, R. Reichle, U. Müller, H. Helm, M. Jungen, and J.A. Stephens, Phys. Rev. A **61**, 033410 (2000).

[48] W. Cencek, J. Rychlewski, R. Jaquet, and W. Kutzelnigg, J. Chem. Phys. **108**, 2831 (1998).

[49] R. Jaquet, W. Cencek, W. Kutzelnigg, and J. Rychlewski, J. Chem. Phys. **108**, 2837 (1998).

[50] F.H. Mies, J. Chem. Phys. **80**, 2514 (1984).

[51] R.H. Dalitz, Philos. Mag. **44**, 1068 (1953).

[52] V. Spirko, P. Jensen, P.R. Bunker, and A. Cejchan, J. Mol. Spectrosc. **112**, 183 (1985).

[53] J.A. Stephens and C.H. Greene, J. Chem. Phys. **103**, 5470 (1995).

[54] O.I. Tolstikhin, V.N. Ostrovsky, and H. Nakamura, Phys. Rev. Lett. **79**, 2026 (1997).

[55] O.I. Tolstikhin, V.N. Ostrovsky, and H. Nakamura, Phys. Rev. A **58**, 2077 (1998).

[56] E.S. Chang and U. Fano, Phys. Rev. A **6**, 173 (1972).

[57] C.M. Lindsay and B.J. McCall, J. Mol. Spectrosc. **210**, 60 (2001).

[58] B.J. McCall, Ph.D. thesis, University of Chicago, 2001 (unpublished).

[59] P. Schiffels, A. Alijah, and J. Hinze, Mol. Phys. **101**, 175 (2003).

[60] P. Schiffels, A. Alijah, and J. Hinze, Mol. Phys. **101**, 189 (2003).

[61] M.C. Bordas, L.J. Lembo, and H. Helm, Phys. Rev. A **44**, 1817 (1991).

[62] M.J. Jensen, H.B. Pedersen, C.P. Safvan, K. Seiersen, X. Urbain, and L.H. Andersen, Phys. Rev. A **63**, 052701 (2001).

[63] T. Tanabe, K. Chida, T. Watanabe, Y. Arakaki, H. Takagi, I. Katayama, Y. Haruyama, M. Saito, I. Nomura, T. Honma, K. Noda, and K. Hoson, in *Dissociative Recombination: Theory, Experiment and Applications IV*, edited by M. Larsson, J.B.A. Mitchell, and I.F. Schneider (World Scientific, Singapore, 2000), p. 170.

[64] T. Tanabe, I. Katayama, H. Kamegaya, K. Chida, Y. Arakaki, T. Watanabe, M. Yoshizawa, M. Saito, Y. Haruyama, K. Hosono, K. Hatanaka, T. Honma, K. Noda, S. Ohtani, and H. Takagi, in *Dissociative Recombination: Theory, Experiment and Applications III*, edited by D. Zaifman, J.B.A. Mitchell, D. Schwalm, and B.R. Rowe (World Scientific, Singapore, 1996), p. 84.

[65] M. Larsson, H. Danared, J.R. Mowat, P. Sigray, G. Sundström, L. Broström, A. Filevich, A. Källberg, S. Mannervik, K.G. Rensfelt, and S. Datz, Phys. Rev. Lett. **70**, 430 (1993).

[66] B.J. McCall, A.J. Huneycutt, R.J. Saykally, T.R. Geballe, N. Djuric, G.H. Dunn, J. Semaniakr, O. Novotny, A. Al-Khalili, A. Ehlerding, F. Hellberg, S. Kalhori, A. Neau, R. Thomas, F. Österdahl, and M. Larsson, Nature (London) **422**, 500 (2003).

[67] T.R. Geballe, Philos. Trans. R. Soc. London, Ser. A **358**, 2503 (2000).

[68] L.H. Andersen and J. Bolko, Phys. Rev. A **42**, 1184 (1990).

[69] H. Kreckel, S. Krohn, L. Lammich, M. Lange, J. Levin, M. Scheffel, D. Schwalm, J. Tennyson, Z. Vager, R. Wester, A. Wolf, and D. Zajfman, Phys. Rev. A **66**, 052509 (2002).

[70] J. Glosík, R. Plası̆ l, V. Poterya, P. Kurdna, and M. Tichý, Chem. Phys. Lett. **331**, 209 (2000).

[71] S. Laubé, A. Le Padellec, O. Sidko, C. Rebrion-Rowe, J.B.A. Mitchell, and B.R. Rowe, J. Phys. B **31**, 2111 (1998).

[72] T. Gougousi, R. Johnsen, and M.F. Golde, Int. J. Mass. Spectrom. **150**, 131 (1995).

[73] M. Larsson, H. Danared, A. Larson, A. Le Padellec, J.R. Peterson, S. Rosen, J. Semaniak, and C. Strömholm, Phys. Rev. Lett. **79**, 395 (1997).

[74] J. Glosík, R. Plası̆ l, V. Poterya, P. Kurdna, M. Tichý, and A. Pysanenko, J. Phys. B **34**, L485 (2001).

[75] R. Plasĭl, J. Glosík, V. Poterya, P. Kurdna, J. Rusz, M. Tichý, and A. Pysanenko, Int. J. Mass. Spectrom. **218**, 105 (2002).

[76] V. Poterya, J. Glosík, R. Plasĭl, M. Tichý, P. Kudrna, and A. Pysanenko, Phys. Rev. Lett. **88**, 044802 (2002).

[77] P. Van der Donk, F.B. Yousif, and J.B.A. Mitchell, Phys. Rev. A **43**, 5971 (1991).